Advanced Composites and Hybrid Materials (2023) 6:207
https://doi.org/10.1007/s42114-023-00790-6

REVIEW

An overview of polymer foaming assisted by supercritical fluid

Mengyao Dong[1] · Gang Wang[1] · Xiangning Zhang[1] · Daqing Tan[1] · Jaya Prasanna Kumar D[2] · Juanna Ren[3,4] · Henry Colorado[5] · Hua Hou[3] · Zhexenbek Toktarbay[6] · Zhanhu Guo[4]

Received: 30 September 2023 / Revised: 30 October 2023 / Accepted: 7 November 2023 / Published online: 14 November 2023

Abstract

In comparison with unfoamed polymers, polymer foams find extensive application in various civil and industrial fields such as packaging, sports equipment, absorbents, and automotive components due to their advantages of lightweight, high strength-to-weight ratio, excellent insulation properties, high thermal stability, high impact strength, toughness, and long fatigue life. The preparation of conventional polymer foam typically necessitates the incorporation of chemical foaming agents into the polymer, raising environmental issues, which pave the way for the utilization of supercritical fluids. Supercritical fluids exemplified by supercritical carbon dioxide or supercritical nitrogen, are renowned for their environmentally friendly and non-toxic characteristics, thus offering a viable alternative to conventional chemical foaming agents. Supercritical fluids exhibit gas-like diffusion and liquid-like density, offering excellent plasticization effects on polymer melts. This substantially reduces the melt viscosity, melting point, and glass transition temperature of the polymer, facilitating the preparation of uniformly distributed, smaller-sized, and higher-density microcellular foams. This review first provides an overview of the characteristics of supercritical fluids and commonly used supercritical fluid foaming agents. Subsequently, the dissolution, diffusion, and interactions of supercritical fluids in polymers were discussed, followed by a focused elucidation of the cell nucleation (homogeneous and heterogeneous) and growth (island model and cell model). Finally, the application of supercritical fluids in the foam manufacturing techniques is highlighted, including batch foaming, extrusion foaming, and injection foaming, while emphasizing the challenges that still exist in polymer foaming.

Keywords Polymer · Foam · Supercritical fluid · Cell nucleation and growth · Foaming technology

✉ Mengyao Dong
dongmy@cqipc.edu.cn

✉ Zhanhu Guo
zhanhu.guo@northumbria.ac.uk

[1] Key Laboratory of Material Processing and Mold Technology, School of Mechanical Engineering and Automation, Chongqing Industry Polytechnic College, Chongqing 401120, China

[2] Department of Chemical Engineering, Ramaiah Institute of Technology, Bengaluru-560054, India

[3] College of Materials Science and Engineering, Taiyuan University of Science and Technology, Taiyuan 030024, China

[4] Integrated Composites Lab (ICL), Department of Mechanical and Construction Engineering, Northumbria University, Newcastle Upon Tyne NE1 8ST, UK

[5] Composites Laboratory, Universidad de Antioquia UdeA, Calle 70 No. 52-21, Medellin, Colombia

[6] Laboratory of Engineering Profile, Satbayev University, Satbayev St. 22a, Almaty 050013, Kazakhstan

1 Introduction

Polymer foam is a kind of solid/gas composite material characterized by a polymer matrix replete with numerous tiny foam holes, commonly referred to as porous polymer material. In contrast to unfoamed polymers, polymer foam exhibits many advantages, including low density, lower thermal conductivity, high impact strength, and lower dielectric constant, etc. [1–4]. Owing to their outstanding functional characteristics and low material cost, polymer foam can be widely used in some fields such as aircraft, automobiles, food packaging, sports equipment, insulation materials, and filter materials [5–14]. In recent years, the increased demand for polymer foam, coupled with its extensive applications, has driven the rapid development of the polymer foam industry.

The conventional approach for preparing polymer foams employs chemical foaming technology [15–20]. Chemical foaming agents, such as azodicarbonamide, p-toluenesulfonyl hydrazine, sodium bicarbonate, and zinc

carbonate, have often been employed in polymer foaming, releasing gases such as carbon dioxide (CO_2) and nitrogen (N_2) upon decomposition by heating. The released gas dissolves within the polymer matrix and initiates bubble nucleation, thereby facilitating the creation of a cellular structure. In addition to adding a chemical blowing agent into the polymer matrix, the inert gases also would be generated by chemical reactions between the two polymers, which can initiate the nucleation and growth of cells. The chemical foaming method has attracted much attention due to its advantages, including cost-effectiveness, simplicity, shortened molding cycles, and the capacity to fabricate large and intricate structural components. However, there are some drawbacks in chemical foaming: firstly, incomplete decomposition of the foaming agent leads to the existence of residues in the resulting foam, restricting its applications, especially in the medical industry. Secondly, the gas generated by chemical foaming is not easy to diffuse uniformly within the polymer, posing challenges in controlling the ultimate cellular structure [21]. The prepared foam material presented inferior cell morphology and non-uniform cell size, which is not conducive to improving the performance of the foam product. Furthermore, chemical foaming agents are detrimental to the human body, resulting in skin, respiratory irritation and allergic reactions [22–24], thus failing to meet green environmental protection standards.

To meet the green, healthy, and pollution-free development, supercritical fluids are being considered as sustainable alternatives for the replacement of the traditional chemical blowing agents during polymer foaming. Supercritical fluids combine the properties of both liquids and gases. They exhibit densities and solvating properties akin to liquids while concurrently possessing diffusivity and viscosity levels on par with gases. The plasticizing effect of supercritical fluid on polymers can drastically reduce the melt viscosity, melting point, and glass transition temperature (T_g) of the polymer, which is conducive to obtaining moderate processing conditions and easy to control over the processing procedure. Polymer foaming with supercritical fluids offers several advantages over chemical foaming, including the absence of organic solvents, non-toxicity, better control of foaming conditions (e.g., temperature and pressure), and the ability to achieve microcellular foam with higher cell density, uniform cell size distribution, and smaller cell size. Consequently, the preparation of polymer foam using the supercritical fluid has emerged as a central research focus. Several articles have been published, covering various topics such as the formation of nanocellular foam [25–27], polymer blend foaming [28, 29], semi-crystalline polymers foaming [30, 31], the foaming of elastomer materials [32–34], engineering plastics and composites foaming [35, 36], and biological materials foaming [37, 38]. Polymer foaming assisted by supercritical fluid constitutes a multifaceted dynamic process necessitating an in-depth grasp of polymer science, physics and chemistry of solutions and interfaces, thermodynamics, and interacting substances, in addition to basic knowledge of process engineering and polymer materials. In this letter, we initially present fundamental insights into supercritical fluids and subsequently delve into a comprehensive analysis of their applications in polymer foaming processes. Lastly, we discussed the research and development of supercritical fluids in foam technology.

2 Supercritical fluids

2.1 Supercritical fluids: definition and properties

The growth of the economy has led to a heightened prominence of environmental concerns. Green chemistry stands out as a vital approach for addressing contemporary environmental challenges. Simultaneously, there is a growing emphasis on adopting a green and health-oriented lifestyle. Consequently, physical foaming agents, particularly supercritical fluids, are progressively supplanting chemical foaming agents [39].

Pure substances undergo state changes, transitioning between gas, liquid, and solid phases as dictated by temperature and pressure. At a specific combination of temperature and pressure, the liquid–gas interface disappears, marking the critical point. Supercritical fluid is characterized as a dense-phase fluid with both pressure and temperature exceeding their respective critical values (see Fig. 1). Under these conditions, the substance presents a behavior between gases and liquids. Specifically, it can permeate solids akin to a gas and dissolve materials in a manner reminiscent of a liquid (see Table 1) [40]. Furthermore, in proximity to the critical point, it is possible to finely adjust the density

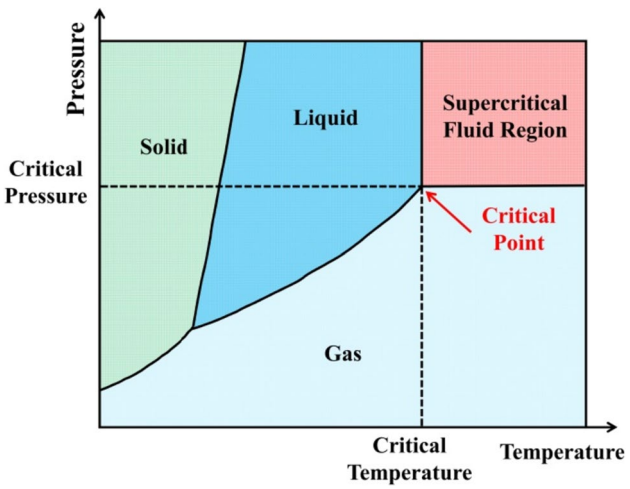

Fig. 1 Typical phase diagram for a pure substance

Table 1 Value Ranges of Density, Viscosity, and Diffusivity for Gas, Supercritical Fluid, and Liquid

Properties	Gas	Supercritical fluid	Liquid
Density (g/L)	0.6–2	100–1000	600–1600
Viscosity (μPa.s)	10–50	10–30	200–3000
Diffusivity $\times 10^{-9}$ (m^2/s)	10,000	10–100	0.2–2

of supercritical fluids through minor alterations in pressure or temperature within the critical region [41]. Table 2 lists the parameters of supercritical fluids of several common substances [40]. Supercritical fluids exhibit low viscosity and nearly zero surface tension. Consequently, they facilitate rapid mass transfer into swollen polymers [42]. Moreover, Supercritical fluids are characterized by their chemical inertness, non-toxicity, and non-flammability [43]. The unique amalgamation of gas-like viscosity and liquid-like density found in the supercritical fluids renders them the outstanding solvents or plasticizers in polymer processing, such as polymer blending, polymer modification, particle production, polymer composites, polymer synthesis, and especially in microcellular foaming [2, 44–47].

2.2 Supercritical carbon dioxide

Currently, supercritical CO_2 represents the predominant foaming agent in supercritical foaming technology, offering the greatest practical potential for development. It serves as the primary compressible fluid capable of facilitating the formation of polymer foam with microcells in both batch and continuous processes [48]. The plasticizing effect of Supercritical CO_2 on polymers can enhance the mobility of polymer chains and reduce the viscosity of polymer melt [49–52] by lowering the T_g or melting temperature (T_m) [53].

Furthermore, CO_2 possesses numerous advantages: (a) Being a component of the atmosphere, CO_2 is cost-effective to obtain and readily available, as it can be directly extracted from the air without causing environmental pollution. (b) It exhibits favorable physical properties, including non-toxicity, chemical stability, and non-flammability. (c) CO_2 stands as the most commonly employed substance, primarily owing to the low critical temperature (31.1 °C) and moderate critical pressure (7.38 MPa), rendering it well-suited for polymer foaming applications.

Supercritical CO_2 foaming technology offers several notable advantages. (a) It does not emit harmful gas, avoiding damage to the environment. (b) Controlling the foaming parameters is straightforward, allowing for precise adjustment of cell size. (c) Supercritical CO_2 exhibits high solubility, robust diffusion capabilities, making it advantageous for producing porous polymer materials with a high nucleation density. (d) CO_2 removal is straightforward and leaves no residual traces [54–58].

Supercritical foaming technology employing supercritical CO_2 as the foaming agent finds extensive application. Firstly, it aids in the extrusion foaming for various applications, including food production and the manufacture of composite materials. Nevertheless, this integrated approach is a recent development and necessitates additional investigation [59]. Secondly, it amalgamates the benefits of processing materials from solvent solutions and supercritical CO_2 batch foaming to create foams with controllable cells while minimizing solvent residues [48]. Thirdly, supercritical CO_2 foaming yields porous silicone rubber foam materials suitable for mechanical energy harvesting. For example, supercritical CO_2 is used in extrusion foaming to produce samples for energy harvesting from tires, while supercritical CO_2 injection foaming is employed to fabricate shoe-shaped samples for capturing energy produced by human motion [57]. Fourthly, supercritical CO_2 is integrated with the elimination of solid porogens to produce drug-loaded scaffolds, addressing the challenge of cell size adjustment druing foaming [56].

Table 2 Critical Conditions of Representative Supercritical Fluids

Solvent	Critical Temperature (°C)	Critical Pressure (bar)
CO_2	31	74
N_2	-147	34
ammonia	132	113
diethyl ether	194	36
hexane	234	30
acetone	235	47
methanol	239	81
ethanol	243	64
toluene	319	41
water	374	221

2.3 Supercritical nitrogen

Supercritical fluid technology utilizing N_2 as the foaming agent encompasses the following characteristics. (a) The resulting polymer foam exhibits a significantly small cell size and a high cell density. (b) This foaming process is environmentally friendly and does not emit toxic gases. (c) N_2 diffuses slowly, reducing the probability of foam collapse after formation. The utilization of supercritical N_2 proves advantageous for foaming elastic materials. Compared to supercritical CO_2, the more uniform cell structure in ethylene-propylene diene monomer (EPDM) rubber profile extrudates was observed when supercritical N_2 was employed as the foaming agent [60]. The foaming behavior of polypropylene (PP) injection molds with N_2 and CO_2 as physical

foaming agents was studied using a visual observation device equipped with temperature and pressure monitoring systems [61]. The results showed that polymer foams with smaller cell size, uniform cell structure and higher cell density employing N_2 as the foaming agent could be obtained, which can ascribed to the lower solubility and higher supersaturation of N_2 within the polymer. In supercritical foaming technology, compared to CO_2, the effectiveness of N_2 as a foaming agent is notably lower, resulting in a relatively higher consumption of N_2. As a result, in practical applications, the cost of using N_2 as the foaming agent surpasses that of utilizing CO_2.

2.4 Co-foamer

Supercritical CO_2 and supercritical N_2 are the predominant foaming agents employed in contemporary supercritical foaming technology, with infrequent utilization of other supercritical fluids. Furthermore, co-foaming agents involving the admixture of supplementary reagents, including ethanol, water, and acetone, with supercritical CO_2 or supercritical N_2 are introduced during the supercritical foaming technology to enhance the foaming ability of plastic materials.

In batch foaming, the effects of ethanol content, temperature, and pressure on the cell structure of polycaprolactone (PCL) were studied by using CO_2 and CO_2-ethanol mixtures, respectively [62]. Compared to supercritical CO_2, a more uniform cell structure was produced with CO_2-ethanol mixtures as the blowing agent. Furthermore, the cell size increases and the cell density decreases with increasing ethanol concentration. The foaming behavior of thermoplastic polyurethane (TPU) was studied by employing CO_2-water as co-foaming agents, and the uniform cell size of the foamed sample was obtained [63]. Salerno et al. utilized a CO_2-ethyl lactate mixture to facilitate the foaming of both PCL and polylactic acid (PLA). The results revealed that incorporating ethyl lactate resulted in a decrease in the operational temperature and enhanced the morphological uniformity of the resulting foam [64]. The foaming behavior of polystyrene (PS) with supercritical CO_2-N_2 as co-foaming agents was explored under elevated temperature and pressure through a visualization system [65]. A synergistic effect was achieved when CO_2 and N_2 were combined at 3:1, which expanded the processing temperature range to achieve a foamed material with the highest cell density. Furthermore, supercritical CO_2 enhances the solubility of supercritical N_2 within PS, leading to an augmented nucleation rate of cells. Consequently, co-foaming agents have the potential to enhance foam properties and hold great promise in the production of high-performance polymer foams [66].

3 Principle of foaming process

The process of polymer foaming typically encompasses the fundamental stages of the formation of a polymer/gas homogeneous system, cell nucleation, and cell growth and stabilization, as shown in Fig. 2.

Under specific temperature and pressure conditions, gas diffuses into the polymer matrix, eventually reaching a state of dissolution equilibrium to create a polymer/gas homogeneously saturated system. The plasticizing effect of gas on polymer can enhance the mobility of the polymer molecular chain, thereby reducing the free energy barrier for cell nucleation. The cell nucleation is driven by thermodynamic instability within the system [67–69]. This instability can be induced by adjusting pressure and temperature during foaming, effectively altering gas solubility in the solution [70, 71]. Once thermodynamic instability occurs, the polymer and gas undergo phase separation, fostering cell nucleation. However, only nuclei that reach a critical size can persist stably. Subsequently, the gas dissolved within the polymer matrix diffuses into the cell nucleus, causing an increase in its diameter. The process of cell growth involves continuous gas consumption and reduction. After a certain period, insufficient gas remains in the system to sustain further cell expansion, leading to a decrease in the driving force for bubble growth. Meanwhile, with decreasing temperature, the viscoelasticity of the polymer melt increases, leading to an increase in resistance to cell growth. Eventually, cell growth stopped and the cell structure and density remained stable. A comprehensive exploration of the foaming mechanism can optimize the processes of polymer foaming, thereby enhancing the performance of polymer foam.

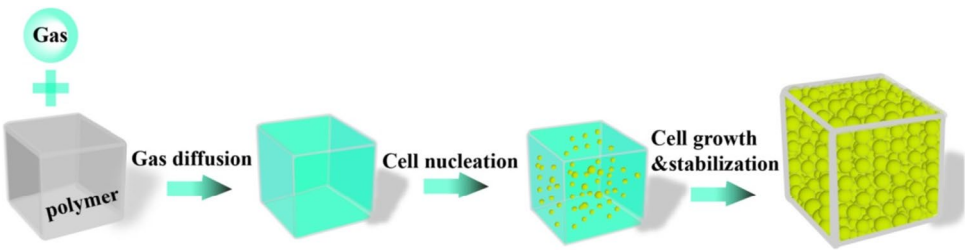

Fig. 2 Schematic diagram of supercritical fluid foaming

3.1 Formation of a polymer/gas homogeneous system

The inert gas (such as CO_2 or N_2) is diffused and dissolved within the polymer under specific temperature and pressure, resulting in the formation of a uniform polymer/gas saturation system. During the saturation phase, the pressure gradient at the polymer matrix surface causes two phenomena: gas dissolution and diffusion within the polymer matrix. The primary foaming agent employed in supercritical foaming technology is supercritical CO_2. Therefore, the discussion was only focused on the dissolution and diffusion of CO_2 within polymer matrix.

3.1.1 Dissolution and diffusion of CO_2 in polymer matrix

Achieving a homogeneous polymer/gas system is pivotal in the foaming process, and it represents a significant challenge in the development of microcellular foaming. Insufficient uniformity results in low cell density and a broader cell size distribution in the final product. To ensure the formation of a homogeneous system, an appropriate quantity of foaming agent should be added to ensure complete dissolution within the polymer melt. Hence, determining gas solubility in polymer melts holds paramount importance.

Solubility measures the quantity of gas absorbed by a material. The concentration of dissolved gas (C) at a given temperature is determined by the pressure (P), as expressed in Eq. (1) [72]:

$$C = S(C)P \tag{1}$$

where S represents the gas solubility. The effect of pressure on the absorption of CO_2 was investigated in polyetherimide (PEI) plaques with a thickness of 1.5 mm [73]. An increase in pressure could potentially raise the maximum solubility of CO_2. Yu et al. studied the dissolution behaviors of CO_2 in PLA melt with the framework of dynamic density functional theory and found that the solubility increases with increasing pressure (see Fig. 3).

The solubility of gas (S) is also temperature-dependent, as outlined by previous studies [77, 78]:

$$S = S_0 e^{\frac{-\Delta H_s}{RT}} \tag{2}$$

where S_0 is the pre-exponential factor, ΔH_s is activation energy for sorption(negative), T is temperature and R is gas constant. Since ΔH_s is negative, the gas solubility decreases with increasing the temperature [79]. Raising the temperature from 40 °C to 150 °C led to a 50% reduction in CO_2 absorption within poly(ethylene glycol), covering saturation pressures ranging from 5 to 15 MPa [80]. Sato [81–83] investigated the solubility of CO_2 in a range of polymers (such as PP, polystyrene (PS), high-density polyethylene (HDPE), etc.) under elevated temperature and pressure conditions. The study revealed that as the temperature increased, the solubility of CO_2 in polymers decreased.

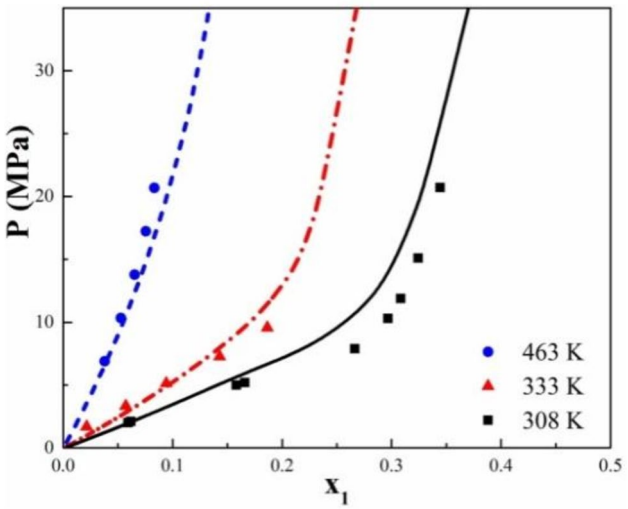

Fig. 3 Solubilities of CO_2 in PLA at various temperatures and pressures. x_1 is the mass fraction (wt%) of CO_2 in PLA melt. The scatter dots at different temperatures (463 k [74], 333 k [75], 308 k [76]) are the experimental data

In most cases, achieving fully saturated polymer/gas systems is imperative for the nano-cell formation process, making the absorption of CO_2 to be a pivotal parameter. Therefore, the adsorption time must be adequate to attain equilibrium between the polymer and gas, which depends on gas diffusion. The temporal progression of the gas concentration distribution is also elucidated using Fick's classical law, as outlined below:

$$\frac{\partial C}{\partial t} = \nabla \cdot D_{12} \nabla C \tag{3}$$

where D_{12} represents the mutual binary diffusion coefficient, reliant not only on the volume fraction of dissolved CO_2 but also on the average hole free volume within the polymer/CO_2 system [84, 85]. According to the free volume theory, temperature and local thermal expansions lead to fluctuations in solvent diffusion within the polymer [86, 87]. The impact of pressure on gas diffusion within polymer materials was emphasized by the free volume theory [88]. Polymer chains have a tendency to constrict under high pressure, restraining free volume. Simultaneously, the gas concentration rises, resulting in an expansion of free volume. For a given temperature, it considers both of these effects, the following relation was proposed:

$$D(P, C) = D_0 e^{\beta P + \alpha C} \tag{4}$$

where D_0 represents a pre-exponential factor, β signifies a negative term associated with the density increase of the polymer matrix, and α is a positive term linked to the

increase of the gas concentration within the polymer matrix. The increasing of free volume in the polymer/CO_2 system enhances solvent diffusion [49]. Similarly, when a solvent is introduced, increasing the system's free volume, the glass transition occurs at a temperature below that of the polymer T_g [87].

3.1.2 Determination of solubility of carbon dioxide in polymers

Researchers have employed various methods to assess the solubility of gas in polymers. The pressure decay method is commonly employed to ascertain gas solubility in polymers due to its simplicity and cost-effective equipment setup. However, the pressure decay method presents challenges when measuring gas solubility in molten polymers, as it necessitates a high-resolution pressure sensor capable of functioning at elevated temperatures. Moreover, this approach demands a sample with a larger size, inevitably extending the measurement duration.

An alternative approach involves employing an electronic balance to directly measure mass increments in adsorption experiments [89, 90]. This method offers rapid measurements and high accuracy. Nonetheless, it is primarily applicable for assessing gas solubility in polymers at lower temperatures due to electronic balance operational constraints. In response, researchers have developed systems to independently control the temperature of the gas absorption chamber and electronic balance [91, 92]. A drawback of this approach is that the change in gas density caused by convection can affect measurement accuracy. Kleinrahm and Wanger introduced a magnetically suspended balance (MSB) to address this issue effectively [93]. In this device, the sample is positioned within a compartment separate from the gas adsorption chamber, allowing to avoid effectively the influence of convection on the mass determination. Consequently, this apparatus can assess gas solubility and diffusivity in polymers under elevated temperature and pressure. Some researchers have embraced this technique to ascertain gas solubility in polymers [83, 94, 95]. Nevertheless, the buoyancy effect of the swollen polymer causes the measured dissolved gas mass (referred to as apparent solubility) by the magnetic levitation balance to be lower than the true solubility.

When precise pressure–volume-temperature data for polymer-gas mixtures is unavailable, researchers commonly employ different equations of state (EOS) to estimate expansion levels to reduce the effects of buoyancy [96, 97]. The Sanchez Lacombe equation of state [98] and Simha Samcynsky equation of state [99] are two widely used equations of state.

3.1.3 Theory on polymer/CO_2 interactions

In solute/solvent systems, solubility is contingent upon the interactions among the constituent components. The Flory–Huggins interaction parameter χ is commonly employed to assess the affinity between solute and solvent [100]. χ is directly proportional to $(\delta_1 - \delta_2)^2$, where δ_1 and δ_2 represent the solubility parameters of components 1 and 2, respectively. When δ_1 and δ_2 exhibit proximity, there is a commensurate increase in the solubility between the constituent components. Therefore, the miscibility can be evaluated through the calculation of solubility parameters δ. Hildebrand and Scott [101] introduced a model grounded in the calculation of cohesive energy density for solute/solvent systems, as indicated by the following equation:

$$\delta = \left(\frac{\Delta E}{V}\right)_T^{0.5} \approx \left(\frac{\partial E}{\partial V}\right)_T^{0.5} = \left(T\left(\frac{\partial P}{\partial T}\right)_V - P\right)^{0.5} \tag{5}$$

where $\Delta E/V$ represents cohesive energy density, P is internal pressure and T signifies temperature. Williams and Colle [102] elucidated this principle in greater detail, demonstrating that supercritical CO_2 exhibits a higher solution parameter than gaseous CO_2, approaching that of hydrocarbon chains (approximately ~ 10 $MPa^{1/2}$). Strauss [103] demonstrated that in the context of a PS/CO_2 system, achieving good gas solubility necessitates the fulfillment of the condition $\delta_1 - \delta_2 < 1$, which mandates the pressure of 90 MPa at 80 °C. However, some studies have evidenced that CO_2 molecules exhibit partial solubility within PS matrices, with solubilities exceeding 13 wt% at pressures below 20 MPa [104, 105]. The phenomenon arises due to the failure of the model to consider the specific chemical interactions.

Another model is grounded in the distribution of interactions among three distinct contributions [106]. By this framework, δ can be deconstructed as follows:

$$\delta^2 = \delta_d^2 + \delta_p^2 + \delta_h^2 \tag{6}$$

where δ_d represents the dispersion component, δ_p denotes the polar component, and δ_h is the hydrogen-bonding component. They can be calculated theoretically based on the consideration of their chemical group contributions, as documented in the available literature [107]. Despite CO_2 lacking a permanent dipole, the substantial influence of its quadrupole moment on interaction is noteworthy, resulting in positive values for δ_p and δ_h within the Hansen model [102]. The finding illustrates the model's constraints. Similar to the Hildebrand and Scott model, the model fails to consider chemical interactions that increase the solubility of gas in polymers [108]. Hence, the gas adsorption behavior varies among different polymers (such as PMMA and PS), contingent upon

their intrinsic properties, even when they share the same T_g. This suggests that distinct molecular compositions of polymers result in varying interactions with CO_2. Extensive research has been conducted on the solubility of block copolymers and fluorinated polymers in CO_2 due to the noteworthy chemical interactions between fluoropolymers and CO_2 [109, 110]. These chemical interactions may exhibit characteristics of Lewis acid–base interactions. Specifically, the fluorine atom serves as a Lewis base alongside the electron-deficient carbon in CO_2. Simultaneously, the hydrogen atoms adjacent to the fluorine atom acquire an induced positive charge and engage with the gaseous oxygen atoms, forming a Lewis acid [111]. Cooper [45] postulated that fluoropolymers create weak complexes with CO_2, resulting in heightened gas solubility within fluoropolymers. Certain silicon-based polymers may be regarded as CO_2-philics polymers. This phenomenon appears to be attributed to the flexibility of the polymer chains [112, 113]. According to Kirby [114] and Nalawade [44], it has been observed that the solubility of CO_2 in poly(dimethyl-) and poly(phenylmethyl-) siloxane exceeds that observed in other polymers, primarily attributable to their notably greater free volume fraction.

Despite being less CO_2-philic than fluoro- or silicon-based polymers, acetate and acrylate polymers are noteworthy due to the significant interaction between their carbonyl groups and CO_2. Especially, PMMA has been extensively investigated for its affinity toward CO_2 in contrast to polyolefins or PS. This affinity can be attributed to carbonyl/gas interactions, similar to the Lewis acid/base interactions observed in fluoro-based polymers, which increase gas solubility [103]. Fourier transform infrared spectroscopy (FT-IR) has been utilized for analyzing these interactions in PMMA, cellulose acetate, and vinyl acetate [115, 116]. Kazarian and colleagues [105] analyze the PMMA/CO_2 interaction by studying the normal vibrational mode v_2 (bending) of CO_2 around 660 cm^{-1}. The spectral band splits into two peaks at 662 and 654 cm^{-1} in PMMA, a phenomenon attributed to interactions between carbonyl groups and gas [44], which is not observed in PS/CO_2 systems [103, 116]. Reglero-Ruiz and colleagues conducted a comparative analysis of CO_2 affinity between PMMA and PS [117]. Their findings demonstrated that PMMA exhibits over a 6 wt% higher gas uptake than PS at 40 °C and 30 MPa.

The affinity between the polymer and CO_2 is a critical factor to consider in the foaming process. Indeed, CO_2-philic polymers enable the attainment of substantial CO_2 absorption at lower saturation pressures and/or shorter durations. Moreover, it is worth noting that the CO_2 solubility can exert an influence on the processes of cell nucleation and growth during polymer foaming.

3.2 Cell nucleation

Nucleation is the phenomenon where molecules from a second phase, previously dissolved in the initial phase, aggregate to establish a stable second phase, driven by thermodynamic instability. Once the supercritical fluid dissolves into the polymer, resulting in the formation of a homogeneous system, the system enters a supersaturated state due to either increased temperature or decreased pressure. The subsequent generation of the bubbles facilitates the attainment of a low-energy stable state. The formation of bubbles in the foaming process can be described by the classical nucleation theory. Colton and Suh et al. [118–120] developed the classical nucleation theory of polymer foaming, widely regarded as the predominant empirical theory for describing the mechanism of cell nucleation.

The assumptions and approximations in classical nucleation theory are as follows [121, 122]: (a) It postulates the nucleus to be a spherical droplet characterized by clearly defined boundaries. (b) All nuclei possess identical physical properties to the bulk material. (c) The theory considers the influence of pressure drop on cell nucleation while disregarding the pressure drop rate. (d) It further postulates that nucleation occurs instantaneously alongside an instantaneous pressure drop, which is unrealistic as pressure drop occurs gradually over time. (e) The bubble interface is similarly described as an infinite, flat planar surface.

Classical nucleation theory has faced challenges due to its underlying assumptions and approximations, leading to significant deviations from experimental observations in some cases, and raising questions about its accuracy and validity [123]. Nonetheless, despite these limitations, classical nucleation theory offers valuable conceptual insights into the nucleation process. Therefore, it is utilized in this paper to elucidate the mechanisms governing bubble nucleation in polymer foams. Classical nucleation theory categorizes cell nucleation into two types: homogeneous nucleation and heterogeneous nucleation.

3.2.1 Homogeneous nucleation

Homogeneous nucleation refers to the spontaneous and stochastic creation of cells within a homogeneous system during the embryo formation stage, without the presence of foreign substances or two-phase incompatible media. It typically arises in reaction to random fluctuations or variations in temperature or pressure. Theoretically, every molecule can potentially serve as a nucleation site, resulting in the most ideal nucleation density and cell radius in homogeneous nucleation. However, due to the absence of induction by nucleating agents, the free energy required for nucleation

is high, which requires the system to have a large degree of supersaturation. During the foaming process, the supersaturated polymer-gas homogeneous system exhibits thermodynamically unstable due to fluctuations in the temperature or pressure, leading to the aggregation of gas molecules. The critical radius (r_c) denotes the minimum size for an embryo to become a stable bubble. A maximum of free energy barrier reaches when the radius of the bubble (R) equals r_c. When the embryo's size falls below r_c, it collapses into the melt. Conversely, when it surpasses r_c, a stable nucleus emerges, persistently growing and causing a decrease in the free energy of the system (see Fig. 4a).

Additionally, bubble stability hinges on the pressure difference ΔP (the disparity between internal bubble pressure and the surrounding pressure) and the interfacial energy, both of which are considered when deriving an expression for Gibbs free energy, as illustrated [124]:

$$\Delta G(R) = -\frac{4}{3}\pi R^3 \Delta P + \pi R^3 \gamma - \Delta V_{\text{free-vol}} \tag{7}$$

where R represents the bubble radius, ΔP is the pressure difference, γ denotes the interfacial tension. $\Delta V_{\text{free-vol}}$ is the change of free volume caused by the additives, which is disregarded in the homogeneous nucleation.

The critical radius r_c depends on the ratio of the interfacial tension γ to the pressure difference ΔP, as shown in the Eq. (8). Therefore, Gibb's free energy barrier ΔG_{Hom} for homogeneous nucleation is expressed by Eq. (9).

$$r_c = \frac{2\gamma}{\Delta P} \tag{8}$$

$$\Delta G_{hom} = \frac{16\pi\gamma^3}{3\Delta P^2} \tag{9}$$

The rate of homogeneous nucleation can be determined by Eq. (10).

$$N_{\text{hom}} = f_0 C_0 \exp\left(\frac{-\Delta G_{hom}}{K_B T}\right) \tag{10}$$

where f_0 represents the frequency factor of the gas molecules attaching to the nucleus and varying with its surface area, C_0 is the concentration of gas molecules, K_B shows the Boltzmann constant; T donates the temperature, ΔG_{hom} stands for the energy barrier associated with homogeneous nucleation.

3.2.2 Heterogeneous nucleation

Heterogeneous nucleation arises when a nucleus forms at the interface between the continuous polymer-gas phase and a third phase, initiated by nucleating agents acting as nucleation centers, rather than spontaneously (see Fig. 4b). Nucleating particles, including fillers [124–134] and crystals [135–140], are frequently employed in both conventional and microcellular foaming processes. They serve to increase nucleation density by offering heterogeneous surfaces that reduce the energy barrier for nucleation [141]. Yu et al. explored the foaming characteristics of the pure poly(L-lactic acid) (PLLA) and PLLA/poly(D-lactic acid) (PDLA) using an environmentally friendly supercritical CO_2 [142]. The result indicates that the stereocomplex crystals can serve

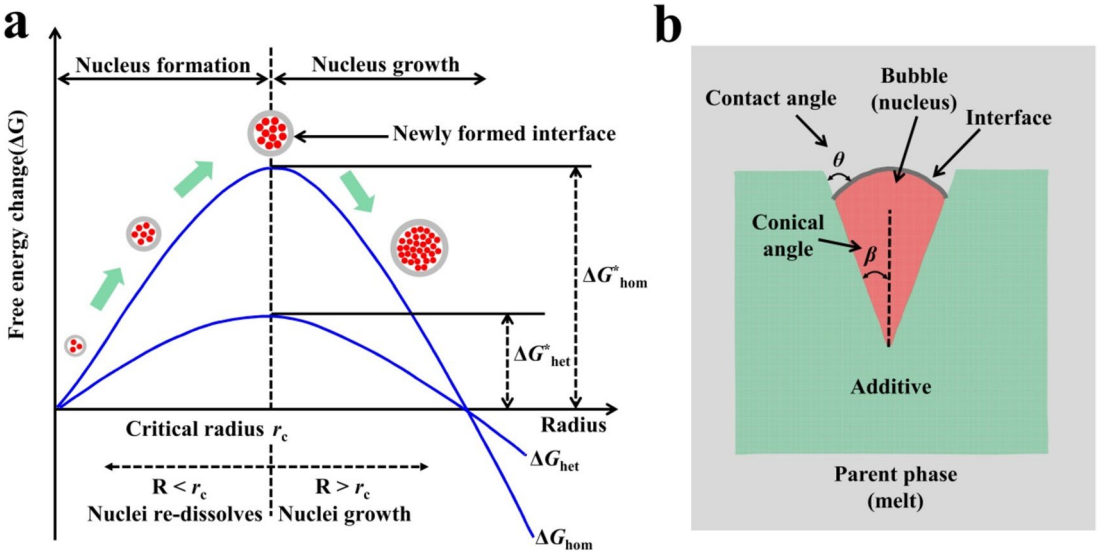

Fig. 4 (**a**) Bubble nucleation and growth as a function of free energy, (**b**) contact angle and semi-conical angle for heterogeneous bubble nucleation

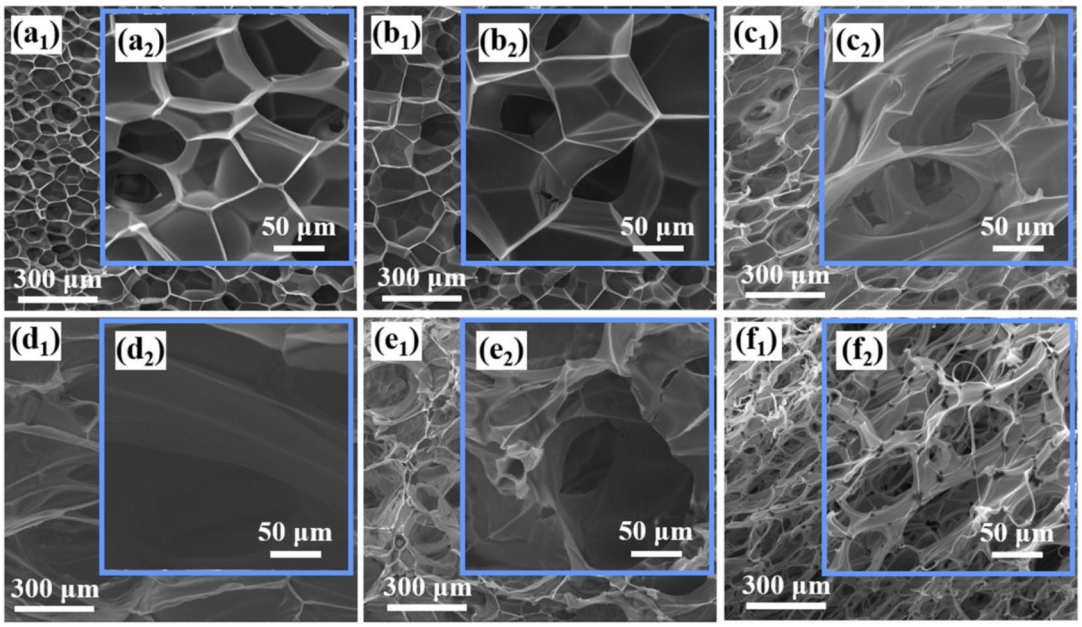

Fig. 5 Cellular morphology of PLLA foams prepared under different foaming temperatures: (**a1**, **a2**) 90 °C; (**b1**, **b2**) 100 °C; (**c1**, **c2**) 105 °C; (**d1**, **d2**) 110 °C; (**e1**, **e2**) 115 °C; (**f1**, **f2**) 120 °C

as nucleation sites, effectively lowering the energy barrier for nucleation, resulting in a remarkable augmentation in cell density and a reduction in cell diameter in PLLA/PDLA foam samples (see Figs. 5, 6, and 7).

Furthermore, the Gibbs free energy maximum is influenced by the surface topography of the nucleating agent, quantified as the shape factor (S). Considering these factors, the expressions of the shape factor were presented in Eqs. (11) and (12).

$$\Delta G_{het} = \Delta G_{hom} S(\theta) \tag{11}$$

$$S(\theta) = \frac{1}{4}\left(2 + 3\cos(\theta) - \cos^2(\theta)\right) \tag{12}$$

Moreover, the determination of the shape factor (S) relies upon the contact angle (θ) established between the bubble radius (R) and the additive surface. As θ increases, S decreases, resulting in further reduction of ΔG_{het}. Notably, some nucleating agents, like talc, do not have a plate-like structure but a particle-like one. For these agents, nucleation occurs within a conically shaped pit, characterized by

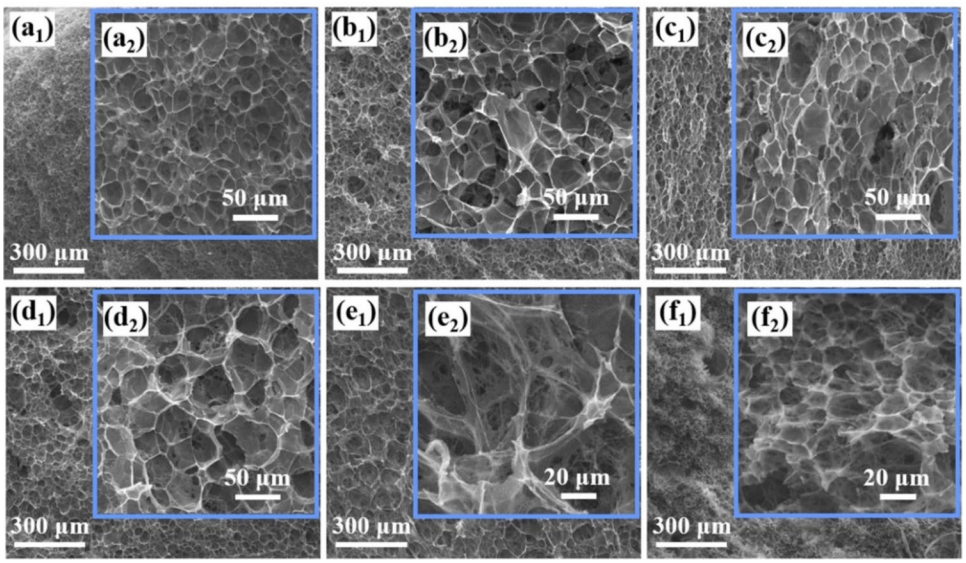

Fig. 6 Cellular morphology of D2.5 foams prepared under different foaming temperatures: (**a1**, **a2**) 90 °C; (**b1**, **b2**) 100 °C; (**c1**, **c2**) 105 °C; (**d1**, **d2**) 110 °C; (**e1**, **e2**) 115 °C; (**f1**, **f2**) 120 °C

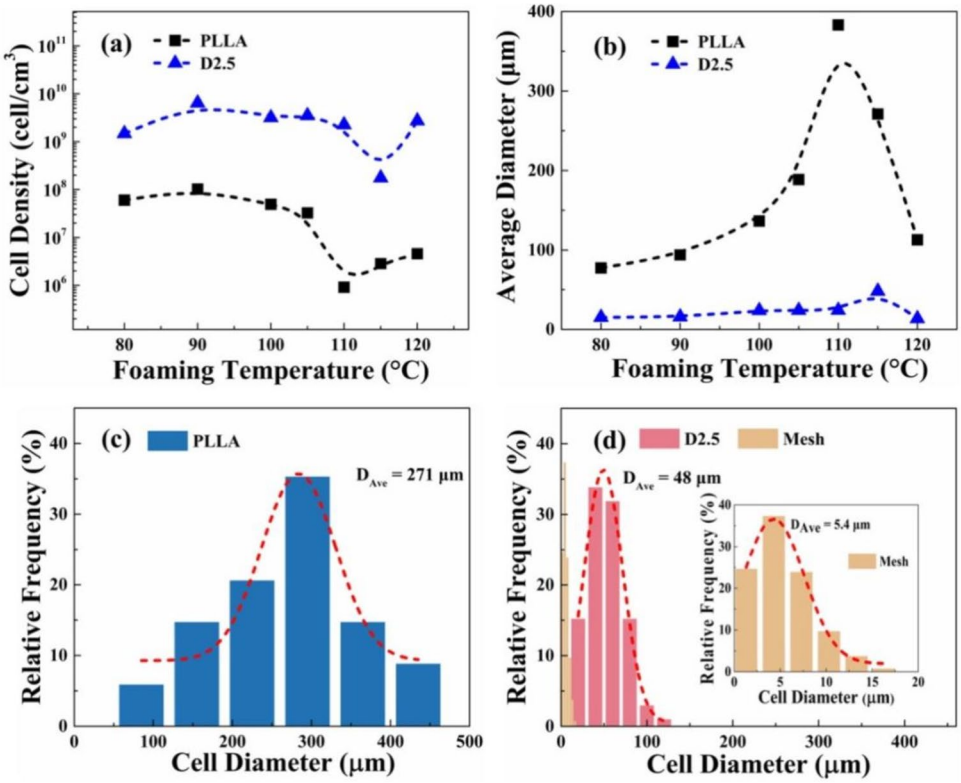

Fig. 7 (**a**) Cell density; (**b**) average diameter of PLLA and D2.5 foams under different foaming temperatures; (**c**) cell size distribution of PLLA foams prepared at 115 °C; (**d**) cell size distribution of D2.5 foams prepared at 115 °C (the insert figure shows the cell size distribution of mesh-like holes)

the semi-conical angle (β) (see Eq. (13)) [143], as illustrated in Fig. 4b.

$$S(\theta,\beta)=\frac{1}{4}\left[-2\sin(\theta-\beta)+\frac{\cos\theta\cos^2(\theta-\beta)}{\sin\beta}\right] \tag{13}$$

Polymer-nucleating agent interactions are of paramount importance in assessing nucleation efficiency. Notably, smaller nucleating agents exhibit a propensity for higher nucleation densities [144, 145]. Besides nucleating agent size, the topography of their surfaces significantly impact nucleation. Compared to tubular nucleating agents, those with flat surfaces demonstrate improved nucleation rates owing to their curved edges [146]. In a study by Leung et al. [147], an exploration was conducted into the impact of both the wetting angle (θ) and the conical cavity angle (β) of nucleating agents. The findings indicated that the difference between these angles ($\theta-\beta$) plays a pivotal role in dictating the growth state of the bubble. ΔG_{het} decreases with increasing θ. Additionally, it has been demonstrated that when $\theta=90°$, a smaller value of β promotes heterogeneous nucleation. Conversely, when θ and β are small, heterogeneous nucleation becomes unfavorable. Hence, an ideal nucleating agent should exhibit uniform size and shape, a large wetting angle, and facile dispersal within a polymer matrix.

3.2.3 Limitations of the classical nucleation theory

While classical nucleation theory delineates the primary parameters governing nucleation, its application to assess nucleation rate in polymer/gas systems frequently diverges from experimental outcomes. Surface tension, dependent on the critical nucleus size, remains inaccessible through experiments. In classical theory, γ is approximated by the surface tension γ_∞ of a planar interface, but this approximation frequently leads to substantial errors. For instance, if the actual surface tension is merely 80% of the planar surface tension, the classical theory may underestimate the nucleation rate by an astonishing 20 orders of magnitude, given a typical free energy barrier of 50 k_BT. In addition, the physical meaning of ΔP is often misunderstood in the literature. While it has been characterized as the pressure difference between the interior and exterior of a bubble, the definition holds only for sufficiently large bubbles [118–120]. Equally critical, internal pressure remains beyond direct measurement. Some researchers have characterized ΔP as the pressure drop required to initiate nucleation, resulting in potential overestimations of ΔP by as much as 30–40%. Such errors could inflate the nucleation rate by several orders of magnitude, reaching levels on the order of 10^9–10^{10}.

In response to this error, new theories have been proposed to improve the accuracy of prediction. One particularly

promising theory is self-consistent field theory. An effective Hamiltonian is introduced in self-consistent field theory, formulated as a straightforward function of a spatially varying field, such as the number density of polymer chain segments, and it incorporates adjustable parameters. By evaluating the associated partition function for this Hamiltonian, it becomes possible to calculate a range of thermodynamic properties. The self-consistent field theory has been effectively employed to model bubble nucleation in the hexadecane-CO_2 system with reasonable accuracy [148]. For the hexadecane-CO_2 model system, Binder and his colleagues observed that classical nucleation theory closely matched self-consistent field theory results in the vicinity of the bimodal region. However, the accuracy of classical nucleation theory diminished for smaller nucleation barriers, which are more representative of experimental conditions.

Statistical-mechanical density functional theory, as described in references [149–154], initiates by constructing a detailed molecular-level model of the system. The associated free energy of this model system is expressed as a function of the spatially varying density distribution of the particles. To minimize the free energy, an equilibrium density distribution was determined. Once the equilibrium distribution is established, the thermodynamic properties of the system can be derived from the function. The statistical-mechanical density functional theory offers a more comprehensive system description compared to self-consistent field theory but demands significantly greater computational resources. Consequently, statistical-mechanical density functional theory and self-consistent field theory complement each other in the study of nucleation and serve as potent tools for addressing the limitations of classical nucleation theory. However, it's important to note that both theories still rely on approximations to facilitate tractable calculations. As such, further experimental investigations are essential to validate and refine these theories.

3.3 Cell growth

The process of bubble growth is highly intricate, encompassing mass, momentum, and heat transfer phenomena. This complexity is further compounded by the intricate rheological behavior of the fluid, making an accurate description of bubble growth challenging. To elucidate the mechanisms governing bubble growth, prior researchers have conducted comprehensive experimental and theoretical investigations, yielding valuable insights.

3.3.1 The bubble radius calculated by the empirical formula

Epstein and Plesset [155] established the correlation between bubble growth and time through an investigation of bubble growth within polymer melts.

$$\frac{dR}{dt} = \alpha\left[\frac{1}{R} + \frac{1}{(\pi Dt)^{\frac{1}{2}}}\right] \tag{14}$$

where R represents the bubble radius; D represents the gas diffusion coefficient; α is a coefficient related to the gas concentration and pressure.

Subsequently, Hobbs [156] investigated the inflation and growth kinetics of bubbles in thermoplastic structural foams. Their model assumes the initial existence of minuscule voids within polymer melt. It takes into account factors such as changes in external pressure, the presence of a range of bubble sizes, and gas diffusion between adjacent bubbles. The research reveals that, under specific pressure conditions, the quantity of expanding bubbles in the molten material relies on the ratio between the critical radius and the average radius of the hypothetical microvoids within the melt. Additionally, it illustrates that the growth rate experiences a notable reduction due to gas diffusion between adjacent bubbles when the inter-bubble separation decreases to a micron or less.

Based on the theory of Epstein [155], an approximate equation for calculating the bubble radius is proposed as follows:

$$R(t) = R_0 + ABt^{\frac{1}{2}} + \frac{(1-A)B^2t}{2R_0 + Bt^{\frac{1}{2}}} \tag{15}$$

where $R(t)$ is the radius of the bubble at time t, R_0 is of the bubble initial radius, A and B are constants associated with the system. The equation takes into account bubble coalescence, providing a more accurate representation of how the bubble radius changes over time. Nevertheless, it is also derived from empirical data and experimental observations, making it challenging to establish a clear relationship between the bubble radius and the parameters influencing bubble expansion. As a result, its application is subject to certain limitations.

3.3.2 "Sea-island" model

The process of bubble growth encompasses both thermodynamics and kinetics, often necessitating computer-based numerical simulations to elucidate the influence of various parameters on bubble expansion [157]. To delve deeper into the mechanism of cell growth, Han and Yoo [158] introduced the sea-island model. This model delineates the expansion of a single bubble within a rectangular cavity immersed in an infinite volume of polymer melt, as depicted in Fig. 8. The model operates under the following assumptions: (a) The bubble remains small during expansion, assuming a spherical shape; (b) Due to the ample width of the cavity, bubble expansion is unrestricted by cavity

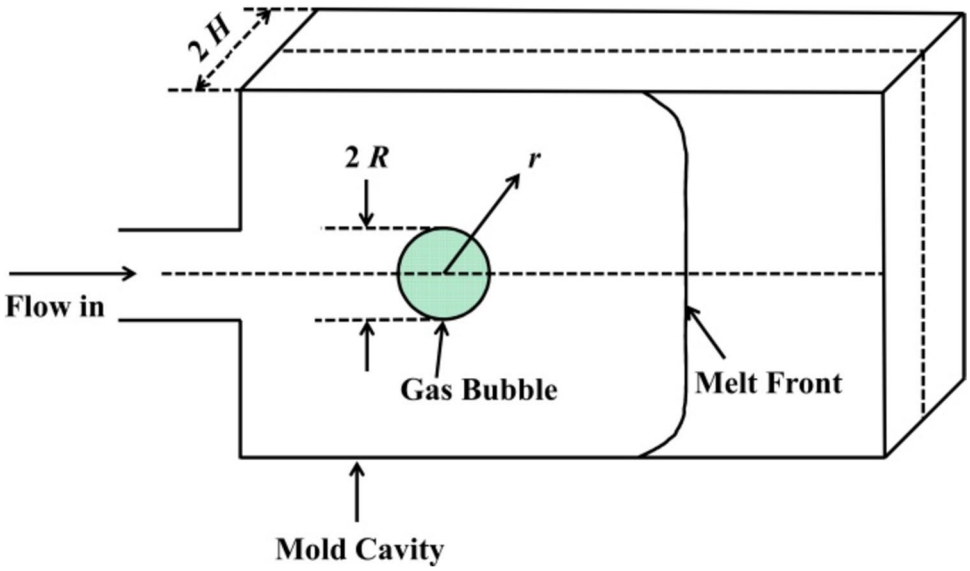

Fig. 8 Island model [158]

walls; (c) Polymer melts exhibit incompressibility; (d) The polymer melt viscosity is exceptionally large, rendering the buoyancy effects during bubble expansion negligible. This model elucidates the growth patterns of bubbles across the entire system by scrutinizing the growth dynamics of individual bubbles. Building upon this concept, Papanstasiou and Scriven [159] employed numerical methods to investigate the growth and rupture of individual spherical bubbles within an infinite volume of polymer melt, grounded in the island model.

In fact, in the real nucleation process, when thermodynamic instability occurs, a large number of bubbles will be generated instantaneously. Given their close proximity, these bubbles experience hindered growth. Therefore, the cell growth process based on the island model will deviate from the actual growth situation, resulting in limited applicability.

3.3.3 Cell model

The growth process of the single bubble in the infinite melt represents the expansion law of bubbles in the entire system, which deviates from reality. Therefore, employing the sea-island model for calculations inevitably introduces errors. To address this, Amon et al. [160] proposed a cell model, where a polymer melt containing numerous bubbles is divided into an equivalent number of blister units. Each cell comprises a spherical bubble core surrounded by a concentric melt shell. In this model, gas in a supersaturated state within the melt shell continuously diffuses into the bubbles, driving their growth, as depicted in Fig. 9. They conducted a study on the diffusion-controlled growth of bubbles enveloped by a Newtonian fluid film using the cell model, simulating the growth of a multitude of bubbles during the foaming process [161]. The cell model accurately reflects the conditions of cell growth and addresses interactions among adjacent bubbles during the growth process, making it widely accepted among researchers.

According to the cell model, the bubble growth kinetics under isothermal conditions can be described by coupled mass and momentum conservation equations. The gas mass conservation in the bubble is expressed as:

$$\frac{d}{dt}\left(\frac{4\pi}{3}\frac{R^3 P_D}{R_g T}\right) = 4\pi R^2 D\frac{\partial c}{\partial r}|r = R \tag{16}$$

The gas mass conservation in the melt can be expressed as:

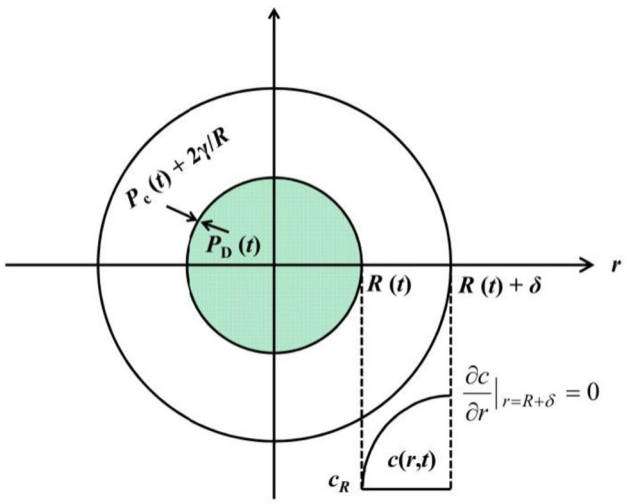

Fig. 9 Schematic of cell model

$$\frac{\partial c}{\partial t}+\frac{RR^2}{r^2}\frac{\partial c}{\partial r}=\frac{D}{r^2}\frac{\partial}{\partial r}\left(r^2\frac{\partial c}{\partial r}\right) \tag{17}$$

The momentum conservation equation is given by:

$$P_D-P_C-\frac{2\gamma}{R}+2\int_R^{\infty}\frac{\sigma_{rr}-\sigma_{\theta\theta}}{r}dr=\frac{4\eta}{R}\left(\frac{dR}{dt}\right) \tag{18}$$

where R is the bubble radius, $R=dR/dt$ is the bubble growth rate, P_D is the pressure inside the bubble, P_C is the pressure of ambient, D is the diffusion coefficient, γ is the interfacial tension, c is the gas concentration, R_g is the gas constant, η is the melt viscosity, and σ is the viscoelastic stress tensor. The viscoelasticity of a polymer is determined by the difference in normal stress $\sigma_{rr}-\sigma_{\theta\theta}$.

The constitutive equation can choose the Oldroyd-B model [49, 162], Larson model [163], Phan-Thien/Tanner (PTT) model [164, 165], and Pom-Pom model [166]. These governing equations for bubble growth dynamics are complex, involving highly coupled nonlinear equations with both partial differential and integral components. The associated boundary conditions are as follows:

$$c(R,0)=k_H P_D(0)=\overline{c}\left(t'\right) \tag{19}$$

Through simulating the bubble growth process, it becomes possible to identify the crucial factors that govern bubble expansion. By adjusting these parameters, the objective of controlling the bubble pore structure can be achieved. While these simulations offer valuable insights into bubble growth kinetics, it's important to note that factors like cell density and cell size distribution may require a comprehensive examination that considers both cell growth kinetics and nucleation processes for accurate determination [167–171].

4 Foam manufacturing techniques

Currently, the production of polymer foam materials can be categorized based on the level of continuous operation into batch foaming, extrusion foaming, and injection molding foaming [172].

4.1 Batch foaming

Batch foaming typically occurs within a high-pressure reactor, creating a controlled, sealed environment with elevated temperature and pressure (see Fig. 10). In this setting, CO_2 or N_2 gradually permeates and dissolves into the polymer matrix. Over time, the gas within the polymer saturates. Subsequently, altering either temperature or pressure induces the gas within the polymer to enter a supersaturated state, resulting in overflow. A large number of bubble nuclei are produced during the overflow process, and the bubble nuclei gradually grow to form cells. Finally, the polymer is cooled, preserving the resulting cell structure within. Batch foaming is typically classified into two categories: temperature-induced and pressure-induced methods.

For the temperature-induced approach [173–176], the initial step involves placing the sample in a low-temperature environment (below T_g) saturated with gas. In this setting, the mobility of the polymer chain is constrained, preventing nucleation. Once saturation is achieved, the sample is removed from the autoclave. Subsequently, the saturated sample is immersed in a high-temperature oil bath for a specified duration, initiating cell nucleation and growth. Elevated temperature (ΔT) serves as the driving force for bubble nucleation. This approach segregates the creation

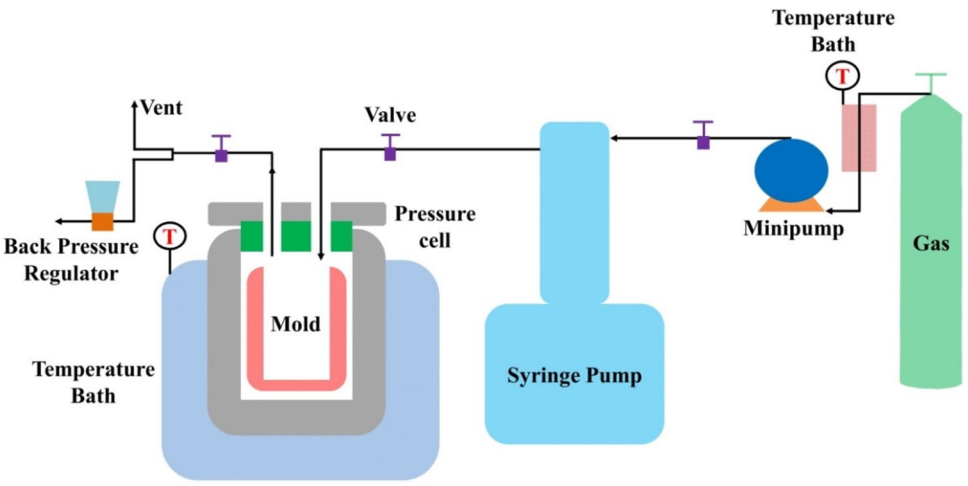

Fig. 10 Schematic representation of batch foaming

of the polymer/gas-saturated system from the subsequent cell nucleation and growth stages, allowing for independent adjustment of process parameters like pressure, temperature, and time. However, this method entails increased complexity and a longer production cycle.

In the temperature-induced process, Miller et al. [73] investigated the foaming behavior of polyetherimide (PEI) sheets saturated for 280 h at 21 °C and 5 MPa. These samples absorbed absorbing 40 wt% CO_2 and underwent foaming in a heated silicone oil bath, resulting in foams with a cell size of 30 nm. Polycarbonate (PC) absorbs approximately 20.4 wt% of CO_2 after saturation at -30 °C for 72 h. Subsequently, it is heated to 70 °C to initiate foaming, resulting in foam with cell size of 21 nm and cell density of 4.1×10^{14} cells/cm^3 [177].

The pressure-induced approach was initially introduced by Goel and Backman [68, 178]. The sample is placed under high-temperature and high-pressure conditions to achieve saturation of CO_2 or N_2 absorption within the polymer sample. Subsequently, the pressure is rapidly reduced, rendering the system thermodynamically unstable and prompting cell nucleation and growth. Costeux [179] utilized the pressure-induced approach to foam PMMA-CO-EMA (a random copolymer of MMA with 50 wt% ethyl methacrylate) copolymers at 30 MPa and 40 °C, resulting in nano-foams with the cell size of 95 nm and the cell density of 8.6×10^{15} cells/cm^3. Yang et al. [180] investigated the foaming behavior of PS-OMS (PS filled with 5 wt% of spherical ordered mesoporous silica) samples through a pressure-induced process. The results revealed that the sample achieved saturation under high pressure at 120 °C for 18 h, and then, the high pressure was swiftly released for 0.5 s, resulting in foam with the average cell size of 7.8 μm and the cell density of 3.55×10^9 cells/cm^3.

Batch foaming techniques provide precise control and are extensively employed for the investigation of diverse process variables. Moreover, the equipment necessary for batch foaming is relatively uncomplicated, and the investment requirement is modest. Nevertheless, its commercial application is constrained due to the incapacity of continuous production.

4.2 Extrusion foaming

Extrusion foaming shares the same operational principles as plastic extrusion, with the primary distinction being the introduction of a physical blowing agent at a specific point along the extrusion line (see Fig. 11). The majority of industrial foam extrusion lines operate in tandem, but single lines are also utilized. Extrusion foaming offers advantages in terms of continuous operation and high output efficiency, making it widely prevalent in industrial production. Initially, polymer pellets or powders are loaded into the temperature-controlled first barrel of the extruder through the hopper.

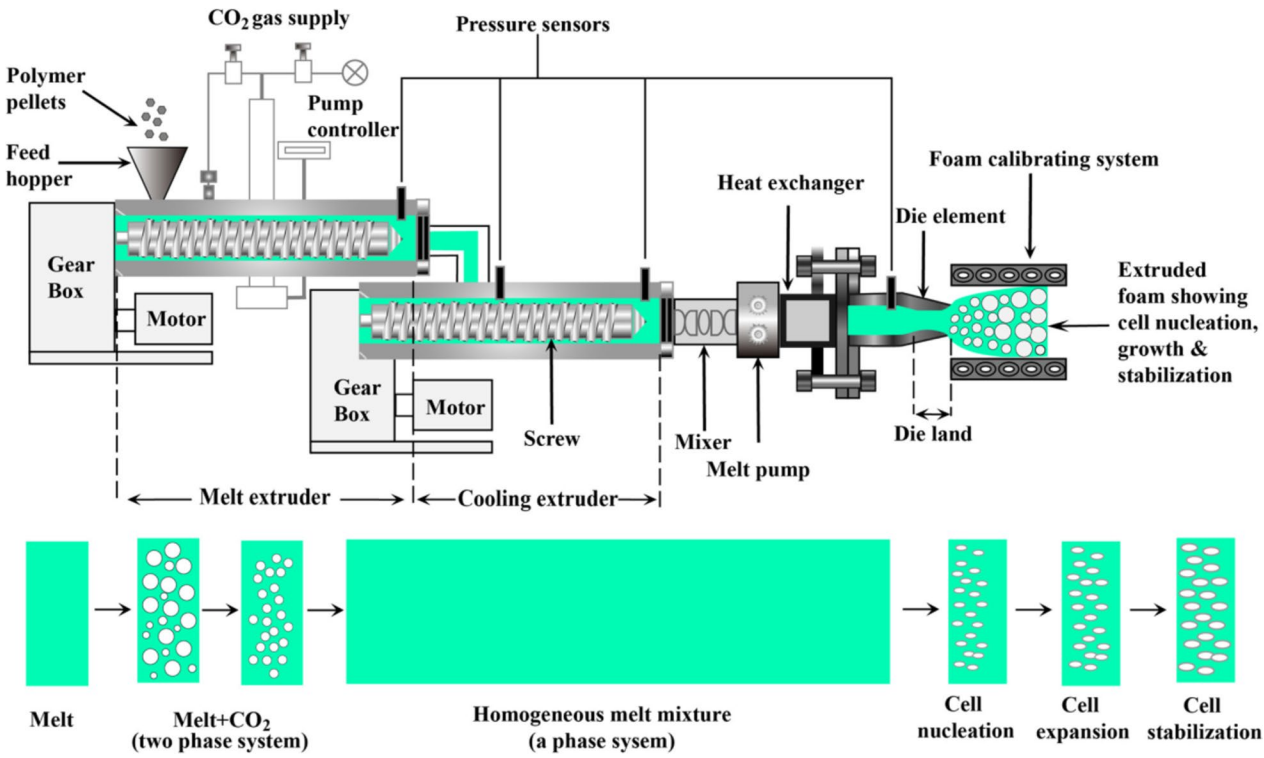

Fig. 11 Schematic representation of foam extrusion on a tandem-line

These pellets undergo melt-plasticization at elevated temperatures and pressures. Subsequently, a physical blowing agent, such as supercritical CO_2, is injected into the melt using an injection unit situated on the barrel. The shearing of the screw accelerates CO_2 diffusion into the polymer melt [181], leading to complete CO_2 dissolution within the polymer melt, resulting in the formation of a homogeneous polymer/CO_2 system.

The homogeneous system is transported to the second barrel via the movement of the screw. The molten material gradually undergoes cooling to a temperature below that of the extruder's first barrel. However, even at this lower temperature, sufficient mixing is still ensured. Cell nucleation is prevented as a result of the high pressure experienced in the barrel. Polymer melt flow rates are regulated by melt pumps, allowing for independent control of flow regardless of temperature and pressure fluctuations. Furthermore, a heat exchanger is employed to provide additional cooling for the homogeneous system. Ultimately, the homogeneous system is conveyed to the extruder head, where pressure is rapidly decreased via a dedicated nozzle. Within this process, CO_2 within the system attains a supersaturated state, escapes from the melt, and initiates nucleation and growth of bubbles. These bubbles continue to expand until vitrification is achieved. Larson and Neldin [182] utilized a 2% epoxy-functional chain extender in masterbatch form to foam PLA, achieving foams with a cell size of 22 µm. Zhang et al. [183] investigated the extrusion foaming of PS using CO_2-water as co-blowing agents. Their experiments employed a throughput of 4 kg/h, a 0.4 mm slot die, and a die temperature of 120 °C, resulting in foams with an average cell diameter of approximately 75 µm when 0.5% graphite (GR) was added as a nucleating agent. Okolieocha et al. [184] conducted a similar study on a tandem foam extrusion line, employing a mixture of carbon dioxide and ethanol as a physical blowing agent (PBA). Their experiments used a 0.5 mm slot die at 126 °C and a throughput of 4.5 kg/h, which yielded foams with a cell size of 25 µm with just 1 wt% TRGO (thermally reduced graphite oxide). Jing Wang et al. [185] investigated the extrusion foaming behavior of PLA with varying molecular weights and branched topologies. They observed that cell density and expansion rate all increased with molecular weight and branching density. For the branched PLA, crystallization enabled stable production of high expansion ratio microcellular foams across a broad temperature range. By controlling crystallinity, it became feasible to produce foams with consistent cell morphology while achieving variations in mechanical properties and surface gloss.

4.3 Injection foaming

Foam injection molding essentially extends the conventional injection molding procedure by incorporating an additional gas injection unit (see Fig. 12). Initially, raw material is introduced into the barrel and directed to the front section of the extruder, where it undergoes melting facilitated by high temperature and screw-driven shearing. Subsequently, gas is introduced into the extruder through a gas injection device, diffusing and dissolving within the melt to establish a homogeneous system. This homogeneous system is

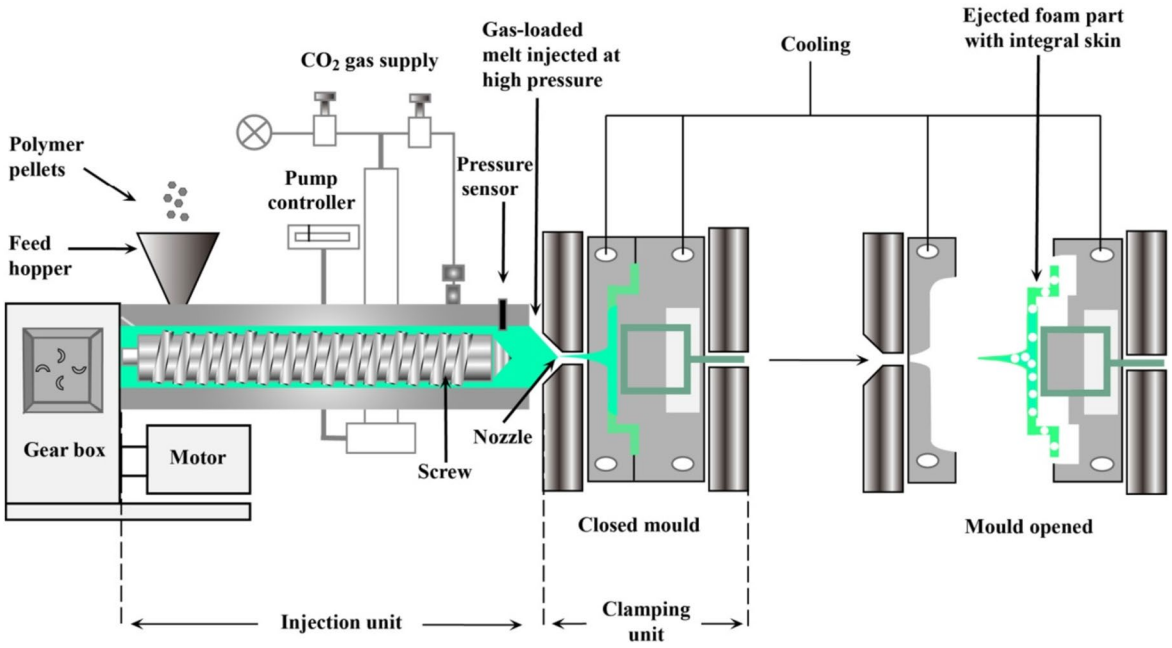

Fig. 12 Schematic representation of foam injection

then transported to a diffusion chamber. Due to the sudden increase in temperature, the solubility of gas in the melt rapidly decreases, inducing a state of supersaturation and initiating nucleation. During this process, the system maintains high pressure to deter premature cell expansion during mold filling. Bubbles commence growth during the depressurization process following mold filling.

Microcellular injection foaming technology stands as one of the prevalent techniques for producing microcellular foam materials, characterized by product cell sizes smaller than those found in traditional foam plastics. These microcells serve to passivate the pre-existing material defects and microcracks, subsequently enhancing plastic strength and, consequently, material mechanical properties. As a result, microcellular injection foaming technology has emerged as a prominent research focus within the field of polymer foam molding.

Li et al. [186] utilized supercritical N_2 to foam polyetherimide with 1 wt% of multiwalled carbon nanotubes, achieving foams characterized by an average cell size of 16.7 μm through the uniform dispersion of multiwalled carbon nanotubes within the polymer matrix. Ming-Cheng Guo et al. [187] investigated the cell structure and mechanical properties of PP foamed samples. They observed that smaller, uniformly distributed cells were attainable with higher injection speeds and lower injection pressures. Tong Lisheng [188–193] employed microcellular injection foaming to prepare PA6-Clay nanocomposites, noting that uniform cell formation was favored by lower melting temperatures, higher gas content, and increased injection speed. Pilla. S and Hwang. S et al. [194–196] delved into the impact of nanoparticle additives on PLA foaming behavior in microcellular injection molding. They reported that the inclusion of nanoparticles enabled the production of foaming materials featuring an average cell diameter ranging from 3 to 40 μm.

5 Conclusions

In the context of growing energy shortages, polymer foam products have garnered significant attention due to their material-saving and cost-effective attributes, coupled with their commendable mechanical and thermal stability, low thermal conductivity, and exceptional dielectric properties. As environmental concerns become increasingly pronounced, green chemistry emerges as a pivotal approach to address environmental and energy challenges. Supercritical foaming technology, as a green technique, aligns more closely with contemporary demands, and consequently, it has found extensive utility in the fabrication of microcellular polymer foam products. Supercritical foaming technology, in comparison to chemical foaming, yields microcellular plastic foam with higher cell densities, smaller cell sizes, and superior comprehensive properties.

Common foaming agents employed in supercritical foaming technology include supercritical CO_2 and supercritical N_2. Supercritical CO_2 exhibits superior solubility and diffusion rates in polymers when compared to supercritical N_2, making it the predominant foaming agent in supercritical foaming technology. When supercritical N_2 is used as a blowing agent, it leads to foams characterized by smaller cell diameters, greater cell densities, and uniform cell sizes. However, in the context of supercritical foaming technology, utilizing N_2 as a foaming agent presents limited success rates, leading to relatively high N_2 consumption. Incorporating co-foaming agents (additional reagents mixed with supercritical CO_2 or supercritical N_2) in supercritical foaming technology can enhance both foaming capacity of sample and the performance of foamed products.

Polymer foaming constitutes a complex dynamic process. To attain foams with high cell density and small cell size, comprehending the gas dissolution and diffusion within the polymer, the mechanisms of cell nucleation and growth, and the requisite foaming conditions is essential. Gas dissolution and diffusion in polymers yield a plasticizing effect, enhancing the fluidity of the polymer matrix, consequently reducing the free energy barrier for cell nucleation and affecting nucleation and growth. The preferred nucleation rates are driven by high thermodynamic instability, stemming from pronounced temperature and pressure gradients, as well as substantial CO_2 absorption. An alternative strategy for controlling nucleation rates and cell growth is to combine various nucleating agents to manipulate the heterogeneous nucleation phenomenon. Additionally, cell growth mechanisms can be elucidated through prior experiments and theoretical investigations.

Batch foaming technology affords precise control and is widely employed for studying the influence of various process parameters (e.g., time, temperature, pressure, and depressurization rate) on polymer foaming behavior. Batch foaming yields uniform cell sizes, enables controlled cell shapes, and results in relatively superior foam performance. However, its limited suitability for continuous production hinders its commercial application. Extrusion foaming offers advantages such as continuous production, high output, and minimal investment, with the additional advantage of unrestricted product length. Injection foam is well-suited for fabricating small, intricate parts in the industrial sector. Notably, there are fewer studies on injection foaming compared to batch and extrusion foaming, possibly attributed to the higher mechanical costs associated with injection foaming.

Researchers have extensively investigated supercritical foaming technology and its mechanisms, achieving significant advancements. Yet, certain topics remain underexplored, including (a) the industrial-scale production of polymer foams; (b) the influence of thermal history on foaming behavior; (c) the effect of rheological properties such as

viscoelasticity and melt strength on foaming behavior; (d) the development of novel foaming agents; (e) the innovation of new foaming techniques. As polymer supercritical foaming technology advances continuously, the overarching trend is to produce highly integrated, precise, and top-quality foam products. By regulating the aggregated structure and morphology of polymer products, foam performance can be elevated to meet evolving product requirements. Diverse, high-quality foam products are poised for broad applications and promising prospects.

Author's contribution Mengyao Dong: Conceived and designed the review, wrote the main text. Gang Wang: Formal analysis and editing. Xiangning Zhang: Formal analysis and editing. Daqing Tan: Data collection and curation. Jaya Prasanna Kumar D: Data collection and curation. Juanna Ren: Data collection and curation. Henry Colorado: Prepared figures and visualization. Hua Hou: Supervision and proofreading the manuscript. Zhexenbek Toktarbay: review and editing. Zhanhu Guo: review and editing.

Funding This work is financially supported by the Natural Science Foundation of Chongqing, China (No. cstc2020jcyj-msxmX1035) and the Doctoral Program of Chongqing, China (No. CSTB2022BSXM-JCX0167). The authors would also like to acknowledge the supports from Youth Project of Science and Technology Research Program of Chongqing Education Commission of China (No.KJQN202103223) and Doctoral Research Fund of Chongqing Industry Polytechnic College (2022GZYBSZK1-08).

Data availability The data will be available upon proper request.

Declarations

Conflict of interest The authors declare no conflict of interest.

References

1. Suh KW, Park CP, Maurer MJ, Tusim MH, Genova RD, Broos R, Sophiea DP (2000) Lightweight cellular plastics. Adv Mater 12(23):1779–1789
2. Tomasko DL, Li H, Liu D, Han X, Wingert MJ, Lee LJ, Koelling KW (2003) A review of CO_2 applications in the processing of polymers. Ind Eng Chem Res 42(25):6431–6456
3. Collias DI, Baird DG, Borggreve RJ (1994) Impact toughening of polycarbonate by microcellular foaming. Polymer 35(18):3978–3983
4. Kumar V (1993) Microcellular polymers: novel materials for the 21st century. Cell Polym 12(3):207–223
5. Krause B, Sijbesma HJP, Münüklü P, van der Vegt NFA, Wessling M (2001) Bicontinuous Nanoporous Polymers by Carbon Dioxide Foaming. Macromolecules 34(25):8792–8801
6. Doroudiani S, Park CB, Kortschot MT (1996) Effect of the crystallinity and morphology on the microcellular foam structure of semicrystalline polymers. Polym Eng Sci 36(21):2645–2662
7. Zhao Y, Hou J, Bai Z, Yang Y, Guo X, Cheng H, Zhao Z, Zhang X, Chen J, Shen C (2020) Facile preparation of lightweight PE/PVDF/Fe_3O_4/CNTs nanocomposite foams with high conductivity for efficient electromagnetic interference shielding. Compos A Appl Sci Manuf 139:106095
8. Jia S, Song S, Zhao X (2021) Selective adsorption and separation of dyes from aqueous solution by a zirconium-based porous framework material. Appl Organomet Chem 35(9):6314
9. Shi G, Yu F, Wang Y, Pan D, Yan X, Li R (2018) Facile synthesis of micro-mesoporous alumina-zirconia nanocrystals with tailoring texture. Chem Phys Lett 709:41–45
10. Zhao X, Zheng M, Gao X, Zhang J, Wang E, Gao Z (2021) The application of MOFs-based materials for antibacterials adsorption. Coord Chem Rev 440:213970
11. Zhao X, Wang Y, Li Y, Xue W, Li J, Wu H, Zhang Y, Li B, Liu W, Gao Z, Huang H (2019) Synergy Effect of Pore Structure and Amount of Carboxyl Site for Effective Removal of Pb2+ in Metal-Organic Frameworks. J Chem Eng Data 64(6):2728–2735
12. Zhao X, Wei Y, Zhao H, Gao Z, Zhang Y, Zhi L, Wang Y, Huang H (2018) Functionalized metal-organic frameworks for effective removal of rocephin in aqueous solutions. J Colloid Interface Sci 514:234–239
13. Wang C, Liu X, Yang T, Sridhar D, Algadi H, Xu BB, El-Bahy ZM, Li H, Ma Y, Li T, Guo Z (2023) An overview of metal-organic frameworks and their magnetic composites for the removal of pollutants. Sep Purif Technol 320:124144
14. Ruan J, Chang Z, Rong H, Alomar TS, Zhu D, AlMasoud N, Liao Y, Zhao R, Zhao X, Li Y, Xu BB, Guo Z, El-Bahy ZM, Li H, Zhang X, Ge S (2023) High-conductivity nickel shells encapsulated wood-derived porous carbon for improved electromagnetic interference shielding. Carbon 213:118208
15. Long Y, An J, Xie X (2020) CO_2-releasing blowing agents from modified polyethylenimines slightly consume isocyanate groups while foaming polyurethanes. Arab J Chem 13(1):3226–3235
16. Ramya G, Crittenden B, Smith M, Camus O, Chew YJ, Perera S (2019) Synthesis of novel regenerable 13X zeolite-polyimide adsorbent foams. Chem Eng J 361:736–750
17. Sadik T, Pillon C, Carrot C, Ruiz JA (2018) Dsc studies on the decomposition of chemical blowing agents based on citric acid and sodium bicarbonate. Thermochim Acta 659:74–81
18. Laguna-Gutierrez E, Escudero J, Rodriguez-Perez MA (2018) Analysis of the mechanical properties and effective diffusion coefficient under static creep loading of low-density foams based on polyethylene/clays nanocomposites. Compos B Eng 148:156–165
19. Sun G, Wang W, Wang L, Yang Z, Liu L, Wang J, Ma N, Wei H, Han S (2017) Effects of aramid honeycomb core on the flame retardance and mechanical property for isocyanate-based polyimide foams. J Appl Polym Sci 134(28):45041
20. Liu C, Long Y, Xie J, Xie X (2017) Towards green polyurethane foams via renewable castor oil-derived polyol and carbon dioxide releasing blowing agents from alkylated polyethylenimines. Polymer 116:240–250
21. Najafi N, Heuzey M-C, Carreau PJ, Therriault D, Park CB (2014) Rheological and foaming behavior of linear and branched polylactides. Rheol Acta 53:779–790
22. Vardar-Sukan F (1998) Foaming: consequences, prevention and destruction. Biotechnol Adv 16(5–6):913–948
23. Hill C, Eastoe J (2017) Foams: From nature to industry. Adv Colloid Interface Sci 247:496–513
24. Schilling K, Zessner M (2011) Foam in the aquatic environment. Water Res 45(15):4355–4366
25. Forest C, Chaumont P, Cassagnau P, Swoboda B, Sonntag P (2015) Polymer nano-foams for insulating applications prepared from CO_2 foaming. Prog Polym Sci 41:122–145
26. Costeux S (2014) CO_2-blown nanocellular foams. J Appl Polym Sci 131(23)
27. Okolieocha C, Raps D, Subramaniam K, Altstädt V (2015) Microcellular to nanocellular polymer foams: Progress (2004–2015) and future directions-A review. Eur Polym J 73:500–519

28. Wan C, Sun G, Gao F, Liu T, Esseghir M, Zhao L, Yuan W (2017) Effect of phase compatibility on the foaming behavior of LDPE/HDPE and LDPE/PP blends with subcritical CO_2 as the blowing agent. J Supercrit Fluids 120:421–431
29. Kong W-L, Bao J-B, Wang J, Hu G-H, Xu Y, Zhao L (2016) Preparation of open-cell polymer foams by CO_2 assisted foaming of polymer blends. Polymer 90:331–341
30. Mi H-Y, Chen J-W, Geng L-H, Chen B-Y, Jing X, Peng X-F (2016) Formation of nanoscale pores in shish-kebab structured isotactic polypropylene by supercritical CO_2 foaming. Mater Lett 167:274–277
31. Tang M, Wang T-C (2017) Foaming of poly(vinylidene fluoride-co-hexafluoropropylene) using supercritical carbon dioxide. J Taiwan Inst Chem Eng 73:146–153
32. Meng L, Liu H, Yu L, Khalid S, Chen L, Jiang T, Li Q (2017) Elastomeric foam prepared by supercritical carbon dioxide. J Appl Polym Sci 134(4)
33. Yoon TJ, Kong W, Kwon DE, Park BK, Lee WI, Lee Y-W (2017) Preparation of solid-state micro- and nanocellular acrylonitrile-butadiene-styrene (ABS) foams using sub- and supercritical CO_2 as blowing agents. J Supercrit Fluids 124:30–37
34. Forest C, Chaumont P, Cassagnau P, Swoboda B, Sonntag P (2015) Generation of nanocellular foams from ABS terpolymers. Eur Polym J 65:209–220
35. Cafiero L, Iannace S, Sorrentino L (2016) Microcellular foams from high performance miscible blends based on PEEK and PEI. Eur Polym J 78:116–128
36. Gedler G, Antunes M, Velasco JI (2016) Low density polycarbonate-graphene nanocomposite foams produced by supercritical carbon dioxide two-step foaming. Thermal stability. Compos Part B Eng 92:299–306
37. Ganjyal G, Reddy N, Yang Y, Hanna M (2004) Biodegradable packaging foams of starch acetate blended with corn stalk fibers. J Appl Polym Sci 93(6):2627–2633
38. Marrazzo C, Maio ED, Iannace S (2007) Foaming of synthetic and natural biodegradable polymers. J Cell Plast 43(2):123–133
39. Villamil Jiménez JA, Le Moigne N, Bénézet JC, Sauceau M, Sescousse R, Fages J (2020) Foaming of PLA composites by supercritical fluid-assisted processes: A review. Molecules 25(15):3408
40. Girard E, Tassaing T, Marty J-D, Destarac M (2016) Structure-Property Relationships in CO_2-philic (Co)polymers: Phase Behavior, Self-Assembly, and Stabilization of Water/CO_2 Emulsions. Chem Rev 116(7):4125–4169
41. Eckert CA, Knutson BL, Debenedetti PG (1996) Supercritical fluids as solvents for chemical and materials processing. Nature 383(6598):313–318
42. Li D, Liu Z, Han B, Song L, Yang G, Jiang T (2002) Preparation of nanometer dispersed polypropylene/polystyrene interpenetrating network using supercritical CO_2 as a swelling agent. Polymer 43(19):5363–5367
43. Zirkel L, Jakob M, Münstedt H (2009) Foaming of thin films of a fluorinated ethylene propylene copolymer using supercritical carbon dioxide. J Supercrit Fluids 49(1):103–110
44. Nalawade SP, Picchioni F, Janssen L (2006) Supercritical carbon dioxide as a green solvent for processing polymer melts: Processing aspects and applications. Prog Polym Sci 31(1):19–43
45. Cooper AI (2000) Polymer synthesis and processing using supercritical carbon dioxide. J Mater Chem 10:207
46. Alsoy S, Duda JL (1999) Processing of polymers with supercritical fluids. Chem Eng Technol: Ind Chem-Plant Equip-Process Eng-Biotechnol 22(11):971–973
47. Kendall JL, Canelas DA, Young JL, DeSimone JM (1999) Polymerizations in supercritical carbon dioxide. Chem Rev 99:543
48. Salerno A, Domingo C (2019) Polycaprolactone foams prepared by supercritical CO_2 batch foaming of polymer/organic solvent solutions. J Supercrit Fluids 143:146–156
49. Chen X, Feng JJ, Bertelo CA (2006) Plasticization effects on bubble growth during polymer foaming. Polym Eng Sci 46(1):97–107
50. Royer JR, DeSimone JM, Khan SA (2001) High-pressure rheology and viscoelastic scaling predictions of polymer melts containing liquid and supercritical carbon dioxide. J Polym Sci Part B: Polym Phys 39(23):3055–3066
51. Royer JR, Gay YJ, Adam M, DeSimone JM, Khan SA (2002) Polymer melt rheology with high-pressure CO_2 using a novel magnetically levitated sphere rheometer. Polymer 43(8):2375–2383
52. Royer JR, Gay YJ, Desimone JM, Khan SA (2000) High-pressure rheology of polystyrene melts plasticized with CO_2: Experimental measurement and predictive scaling relationships. J Polym Sci Part B: Polym Phys 38(23):3168–3180
53. Areerat S, Funami E, Hayata Y, Nakagawa D, Ohshima M (2004) Measurement and prediction of diffusion coefficients of supercritical CO_2 in molten polymers. Polym Eng Sci 44(10):1915–1924
54. Duarte ARC, Mano JF, Reis RL (2009) Supercritical fluids in biomedical and tissue engineering applications: a review. Int Mater Rev 54(4):214–222
55. Li Y, Gong P, Liu Y, Niu Y, Park CB, Li G (2021) Environmentally friendly and zero-formamide EVA/LDPE microcellular foams via supercritical carbon dioxide solid foaming. ACS Appl Polym Mater 3(8):4213–4222
56. Santos-Rosales V, Ardao I, Goimil L, Gomez-Amoza JL, García-González CA (2021) Solvent-free processing of drug-loaded poly (ε-caprolactone) scaffolds with tunable macroporosity by combination of supercritical foaming and thermal porogen leaching. Polymers 13(1):159
57. Shao Y, Luo C, Deng B-W, Yin B, Yang M-B (2020) Flexible porous silicone rubber-nanofiber nanocomposites generated by supercritical carbon dioxide foaming for harvesting mechanical energy. Nano Energy 67:104290
58. Sun L, Gao M, Tang S (2021) Porous amino acid-functionalized poly(ionic liquid) foamed with supercritical CO_2 and its application in CO_2 adsorption. Chem Eng J 412:128764
59. Sauceau M, Fages J, Common A, Nikitine C, Rodier E (2011) New challenges in polymer foaming: A review of extrusion processes assisted by supercritical carbon dioxide. Prog Polym Sci 36(6):749–766
60. Michaeli W, Westermann K, Sitz S (2011) Extrusion of physically foamed rubber profiles. J Cell Plast 47(5):483–495
61. Ishikawa T, Taki K, Ohshima M (2012) Visual observation and numerical studies of N_2 vs. CO_2 foaming behavior in core-back foam injection molding. Polym Eng Sci 52(4):875–883
62. Tsivintzelis I, Pavlidou E, Panayiotou C (2007) Biodegradable polymer foams prepared with supercritical CO_2-ethanol mixtures as blowing agents. J Supercrit Fluids 42(2):265–272
63. Mi HY, Jing X, Salick MR, Peng XF, Turng LS (2014) A novel thermoplastic polyurethane scaffold fabrication method based on injection foaming with water and supercritical carbon dioxide as coblowing agents. Polym Eng Sci 54(12):2947–2957
64. Hu D-D, Gu Y, Liu T, Zhao L (2018) Microcellular foaming of polysulfones in supercritical CO_2 and the effect of co-blowing agent. J Supercrit Fluids 140:21–31
65. Wong A, Mark LH, Hasan MM, Park CB (2014) The synergy of supercritical CO_2 and supercritical N_2 in foaming of polystyrene for cell nucleation. J Supercrit Fluids 90:35–43
66. Feng D, Li L, Wang Q (2019) Fabrication of three-dimensional polyetherimide bead foams via supercritical CO_2/ethanol co-foaming technology. RSC Adv 9(7):4072–4081

67. Tsivintzelis I, Sanxaridou G, Pavlidou E, Panayiotou C (2016) Foaming of polymers with supercritical fluids: A thermodynamic investigation. J Supercrit Fluids 110:240–250
68. Goel SK, Beckman EJ (1994) Generation of microcellular polymeric foams using supercritical carbon dioxide. I: Effect of pressure and temperature on nucleation. Polym Eng Sci 34(14):1137–1147
69. Frank X, Dietrich N, Wu J, Barraud R, Li HZ (2007) Bubble nucleation and growth in fluids. Chem Eng Sci 62(24):7090–7097
70. Thompson RB, Park CB, Chen P (2010) Reduction of polymer surface tension by crystallized polymer nanoparticles. J Chem Phys 133(14)
71. Panploo K, Chalermsinsuwan B, Poompradub S (2019) Natural rubber latex foam with particulate fillers for carbon dioxide adsorption and regeneration. RSC Adv 9(50):28916–28923
72. Klopffer M, Flaconneche B (2001) Transport properties of gases in polymers: bibliographic review. Oil Gas Sci Technol 56(3):223–244
73. Miller D, Chatchaisucha P, Kumar V (2009) Microcellular and nanocellular solid-state polyetherimide (PEI) foams using sub-critical carbon dioxide I. Processing and structure. Polymer 50(23):5576–5584
74. Mahmood SH, Keshtkar M, Park CB (2014) Determination of carbon dioxide solubility in polylactide acid with accurate PVT properties. J Chem Thermodyn 70:13–23
75. Liu D, Tomasko DL (2007) Carbon dioxide sorption and dilation of poly(lactide-co-glycolide). J Supercrit Fluids 39(3):416–425
76. Pini R, Storti G, Mazzotti M, Tai H, Shakesheff KM, Howdle SM (2008) Sorption and swelling of poly (DL-lactic acid) and poly (lactic-co-glycolic acid) in supercritical CO_2: An experimental and modeling study. J Polym Sci Part B: Polym Phys 46(5):483–496
77. Handa YP, Zhang Z, Wong B (2001) Solubility, Diffusivity, and Retrograde Vitrification in PMMA-CO_2, and Development of Sub-micron Cellular Structures. Cell Polym 20(1):1–16
78. Marchese J, Garis E, Anson M, Ochoa NA, Pagliero C (2003) Gas sorption, permeation and separation of ABS copolymer membrane. J Membr Sci 221(1):185–197
79. Pantoula M, Panayiotou C (2006) Sorption and swelling in glassy polymer/carbon dioxide systems: Part I Sorption. J Supercrit Fluids 37(2):254–262
80. Vitoux P, Tassaing T, Cansell F, Marre S, Aymonier C (2009) In Situ IR Spectroscopy and Ab Initio Calculations To Study Polymer Swelling by Supercritical CO_2. J Phys Chem B 113:897
81. Sato Y, Fujiwara K, Takikawa T, Takishima S, Masuoka H (1999) Solubilities and diffusion coefficients of carbon dioxide and nitrogen in polypropylene, high-density polyethylene, and polystyrene under high pressures and temperatures. Fluid Phase Equilib 162(1):261–276
82. Sato Y, Yurugi M, Fujiwara K, Takishima S, Masuoka H (1996) Solubilities of carbon dioxide and nitrogen in polystyrene under high temperature and pressure. Fluid Phase Equilib 125(1):129–138
83. Sato Y, Takikawa T, Takishima S, Masuoka H (2001) Solubilities and diffusion coefficients of carbon dioxide in poly(vinyl acetate) and polystyrene. J Supercrit Fluids 19(2):187–198
84. Cohen MH, Turnbull D (1959) Molecular transport in liquids and glasses. J Chem Phys 31(5):1164–1169
85. Vrentas JS, Duda JL (1977) Diffusion in polymer-solvent systems. I. Reexamination of the free-volume theory. J Polym Sci Polym Phys Ed 15(3):403–416
86. Vrentas JS, Vrentas CM (1994) Solvent Self-Diffusion in Glassy Polymer-Solvent Systems. Macromolecules 27(20):5570–5576
87. Vrentas JS, Vrentas CM (1994) Solvent Self-Diffusion in Rubbery Polymer-Solvent Systems. Macromolecules 27(17):4684–4690
88. Naito Y, Kamiya Y, Terada K, Mizoguchi K, Wang JS (1996) Pressure dependence of gas permeability in a rubbery polymer. J Appl Polym Sci 61(6):945–950
89. Kamiya Y, Mizoguchi K, Naito Y, Hirose T (1986) Gas sorption in poly (vinyl benzoate). J Polym Sci Part B: Polym Phys 24(3):535–547
90. Wong B, Zhang Z, Handa YP (1998) High-precision gravimetric technique for determining the solubility and diffusivity of gases in polymers. J Polym Sci Part B: Polym Phys 36(12):2025–2032
91. Kamiya Y, Mizoguchi K, Terada K, Fujiwara Y, Wang J-S (1998) CO_2 Sorption and Dilation of Poly(methyl methacrylate). Macromolecules 31(2):472–478
92. Lee JG, Flumerfelt RW (1995) Nitrogen solubilities in low-density polyethylene at high temperatures and high pressures. J Appl Polym Sci 58(12):2213–2219
93. Kleinrahm R, Wagner W (1986) Measurement and correlation of the equilibrium liquid and vapour densities and the vapour pressure along the coexistence curve of methane. J Chem Thermodyn 18(8):739–760
94. Areerat S, Hayata Y, Katsumoto R, Kegasawa T, Egami H, Ohshima M (2002) Solubility of carbon dioxide in polyethylene/titanium dioxide composite under high pressure and temperature. J Appl Polym Sci 86(2):282–288
95. Li G, Li H, Wang J, Park C (2006) Investigating the solubility of CO_2 in polypropylene using various EOS models. Cell Polym 25(4):237–248
96. Li G, Gunkel F, Wang J, Park C, Altstädt V (2007) Solubility measurements of N_2 and CO_2 in polypropylene and ethene/octene copolymer. J Appl Polym Sci 103(5):2945–2953
97. Xie H, Simha R (1997) Theory of solubility of gases in polymers. Polym Int 44(3):348–355
98. Sanchez IC, Lacombe RH (1978) Statistical thermodynamics of polymer solutions. Macromolecules 11(6):1145–1156
99. Simha R, Somcynsky T (1969) On the statistical thermodynamics of spherical and chain molecule fluids. Macromolecules 2(4):342–350
100. Flory PJ (1953) Principles of polymer chemistry, Cornell university press
101. Hildebrand J, Scott R (1950) The Solubility of Nonelectrolytes, third edit. Reinhold, New York
102. Williams LL, Rubin JB, Edwards HW (2004) Calculation of hansen solubility parameter values for a range of pressure and temperature conditions including the supercritical fluid region. Ind Eng Chem Res 43(16):4967–4972
103. Strauss W, D'Souza NA (2004) Supercritical CO_2 processed polystyrene nanocomposite foams. J Cell Plast 40(3):229–241
104. Garcia-Leiner M, Lesser AJ (2004) CO_2-assisted polymer processing: A new alternative for intractable polymers. J Appl Polym Sci 93(4):1501–1511
105. Kazarian SG, Vincent MF, Bright FV, Liotta CL, Eckert CA (1996) Specific Intermolecular Interaction of Carbon Dioxide with Polymers. J Am Chem Soc 118:1729
106. Hansen CM (2004) Aspects of solubility, surfaces and diffusion in polymers. Prog Org Coat 51(1):55–66
107. Lindvig T, Michelsen ML, Kontogeorgis GM (2002) A Flory-Huggins model based on the Hansen solubility parameters. Fluid Phase Equilib 203(1):247–260
108. Kasturirangan A, Koh CA, Teja AS (2011) Glass-Transition Temperatures in CO_2 + Polymer Systems: Modeling and Experiment. Ind Eng Chem Res 50(1):158–162
109. Andre P, Lacroix-Desmazes P, Taylor DK, Boutevin B (2006) Solubility of fluorinated homopolymer and block copolymer in compressed CO_2. J Supercrit Fluids 37:263
110. Ribaut T, Oberdisse J, Annighofer B, Fournel B, Sarrade S, Haller H, Lacroix-Desmazes P (2011) Solubility and Self-Assembly of Amphiphilic Gradient and Block Copolymers in Supercritical CO_2. J Phys Chem B 115:836

111. Kilic S, Michalik S, Wang Y, Johnson JK, Enick RM, Beckman EJ (2007) Phase Behavior of Oxygen-Containing Polymers in CO_2. Macromolecules 40:1332
112. Fink R, Hancu D, Valentine R, Beckman EJ (1999) Toward the Development of "CO_2-philic" Hydrocarbons. 1. Use of Side-Chain Functionalization to Lower the Miscibility Pressure of Polydimethylsiloxanes in CO_2. J Phys Chem B 103(31):6441–6444
113. Kilic S, Wang Y, Johnson JK, Beckman EJ, Enick RM (2009) Influence of tert-amine groups on the solubility of polymers in CO_2. Polymer 50:2436
114. Kirby CF, McHugh MA (1999) Phase behavior of polymers in supercritical fluid solvents. Chem Rev 99(2):565–602
115. Fried J, Li W (1990) High-pressure FTIR studies of gas-polymer interactions. J Appl Polym Sci 41(5–6):1123–1131
116. Shieh Y-T, Liu K-H (2003) The effect of carbonyl group on sorption of CO_2 in glassy polymers. J Supercrit Fluids 25(3):261–268
117. Reglero JA, Viot P, Dumon M (2011) Foaming of amorphous polymers and blends in supercritical CO_2: Solubility versus block copolymers addition. J Cell Plast 47(6):535–548
118. Colton J, Suh N (1987) The nucleation of microcellular thermoplastic foam with additives: Part I: Theoretical considerations. Polym Eng Sci 27(7):485–492
119. Colton J, Suh N (1987) The nucleation of microcellular thermoplastic foam with additives: Part II: Experimental results and discussion. Polym Eng Sci 27(7):493–499
120. Colton JS, Suh NP (1987) Nucleation of microcellular foam: Theory and practice. Polym Eng Sci 27(7):500–503
121. Kim Y, Park CB, Chen P, Thompson RB (2011) Origins of the failure of classical nucleation theory for nanocellular polymer foams. Soft Matter 7(16):7351–7358
122. Oxtoby DW (1998) Nucleation of first-order phase transitions. Acc Chem Res 31(2):91–97
123. Xu X, Cristancho DE, Costeux S, Wang Z-G (2013) Bubble nucleation in polymer-CO_2 mixtures. Soft Matter 9(40):9675–9683
124. Costeux S, Khan I, Bunker SP, Jeon HK (2015) Experimental study and modeling of nanofoams formation from single phase acrylic copolymers. J Cell Plast 51(2):197–221
125. Di Y, Iannace S, Maio ED, Nicolais L (2005) Poly (lactic acid)/organoclay nanocomposites: thermal, rheological properties and foam processing. J Polym Sci Part B: Polym Phys 43(6):689–698
126. Jin W, Xingguo C, Mingjun Y, Jiasong H (2001) An investigation on the microcellular structure of polystyrene/LCP blends prepared by using supercritical carbon dioxide. Polymer 42(19):8265–8275
127. Shen J, Zeng C, Lee LJ (2005) Synthesis of polystyrene-carbon nanofibers nanocomposite foams. Polymer 46(14):5218–5224
128. Yu K, Jiang H, Zhou H, Mi J, He Y, Wang X (2018) Evolution of double crystal melting peak in polypropylene foam assisted by β-nucleating agent and supercritical CO_2. J Appl Polym Sci 135(12):46007
129. Fu L, Li K, Qin H, Hou J, Zhang X, He G, Liu B, Ren C, Chen J (2022) Sandwich structured iPP/CNTs nanocomposite foams with high electromagnetic interference shielding performance. Compos Sci Technol 220:109297
130. Zuo K, Xu J, Xie S, Zhang S, Hou J, Yang Y, Zhang X, Chen J (2021) Microcellular foaming and mechanical properties of iPPF reinforced PPR composites. J Supercrit Fluids 170:105161
131. Zhang X, Wang X, Dong B, Zheng G, Chen J, Shen C, Park CB (2021) Synergetic effect of crystal nucleating agent and melt self-enhancement of isotactic polypropylene on its rheological and microcellular foaming properties. J Cell Plast 57(1):101–121
132. Wang B, Lin F-H, Li X-Y, Ji X-R, Liu S-X, Han X-J, Yuan Z-Q, Luo J (2019) Transcrystallization of isotactic polypropylene/bacterial cellulose hamburger composite. Polymers 11(3):508
133. Wang B, Lin F-H, Li X-Y, Zhang Z-W, Xue X-R, Liu S-X, Ji X-R, Yu Q, Yuan Z-Q, Chen X-D (2018) Isothermal crystallization and rheology properties of isotactic polypropylene/bacterial cellulose composite. Polymers 10(11):1284
134. Gao C, Liao J, Lu J, Ma J, Kianfar E (2021) The effect of nanoparticles on gas permeability with polyimide membranes and network hybrid membranes: a review. Rev Inorg Chem 41(1):1–20
135. Baldwin DF, Park CB, Suh NP (1996) A microcellular processing study of poly (ethylene terephthalate) in the amorphous and semicrystalline states. Part I: Microcell nucleation. Polym Eng Sci 36(11):1437–1445
136. Taki K, Kitano D, Ohshima M (2011) Effect of Growing Crystalline Phase on Bubble Nucleation in Poly(L-Lactide)/CO_2 Batch Foaming. Ind Eng Chem Res 50(6):3247–3252
137. Yu K, Wang D, Hou J, Zhang X, Chen J (2023) Fabrication of poly(lactic acid) foam with high expansion ratio and oriented cellular structure by restricting cold crystallization. Int J Biol Macromol 251:126463
138. Fu L, Shi Q, Ji Y, Wang G, Zhang X, Chen J, Shen C, Park CB (2020) Improved cell nucleating effect of partially melted crystal structure to enhance the microcellular foaming and impact properties of isotactic polypropylene. J Supercrit Fluids 160:104794
139. Zhang X, Li B, Wang X, Li K, Wang G, Chen J, Park CB (2018) Modification of iPP microcellular foaming behavior by thermal history control and nucleating agent at compressed CO_2. J Supercrit Fluids 133:383–392
140. Wang B, Lin F-H, Zhao Y-Y, Li X-Y, Liu Y-C, Li J-B, Han X-J, Liu S-X, Ji X-R, Luo J (2019) Isotactic polybutene-1/bamboo powder composites with excellent properties at initial stage of molding. Polymers 11(12):1981
141. Wang B, Zhang H-R, Huang C, Xiong L, Luo J (2017) Study on non-isothermal crystallization behavior of isotactic polypropylene/bacterial cellulose composites. RSC Adv 7(67):42113–42122
142. Yu K, Wu Y, Zhang X, Hou J, Chen J (2022) Microcellular open-cell poly (L-lactic acid)/poly (D-lactic acid) foams for oil-water separation prepared via supercritical CO_2 foaming. J CO_2 Util 65:102219
143. Park CB, Cheung LK, Song S-W (1998) The effect of talc on cell nucleation in extrusion foam processing of polypropylene with CO_2 and isopentane. Cell Polym 17(4):221–251
144. Chen L, Blizard K, Straff R, Wang X (2002) Effect of filler size on cell nucleation during foaming process. J Cell Plast 38(2):139–148
145. Ramesh N, Lee S (2005) Do nanoparticles really assist in nucleation of fine cells in polyolefin foams? Cell Polym 24(5):269–277
146. Fletcher NH (1958) Size effect in heterogeneous nucleation. J Chem Phys 29(3):572–576
147. Leung SN, Park CB, Li H (2010) Effects of nucleating agents' shapes and interfacial properties on cell nucleation. J Cell Plast 46(5):441–460
148. Müller M, MacDowell L, Virnau P, Binder K (2002) Interface properties and bubble nucleation in compressible mixtures containing polymers. J Chem Phys 117(11):5480–5496
149. Yu K, Zhou H, Wang X, Du Z, Mi J (2019) From thermodynamics to kinetics: Theoretical study of CO_2 dissolving in poly (lactic acid) melt. J Mol Liq 280:97–103
150. Yu K, Ni J, Zhou H, Wang X, Mi J (2020) Effects of in-situ crystallization on poly (lactic acid) microcellular foaming: Density functional theory and experiment. Polymer 200:122539
151. Ren R-R, Lv C-Q, Liu J-H, Wang G-C (2022) Investigation of the oxygen coverage of propylene epoxidation on Ag(111) surfaces from DFT. Comput Theor Chem 1214:113739
152. Zhang J, Yang J, Cheng L, Wang Y, Feng G (2020) Adsorption of acetylene on Sn-doped Ni (111) surfaces: a density functional study. J Mol Model 26:1–8
153. Zhang J, Wang Y, Wang Y, Zhang M (2017) Catalytic activity for oxygen reduction reaction on CoN_2 embedded

graphene: a density functional theory study. J Electrochem Soc 164(12):F1122
154. Zhi C, Wang Q, Wang B, Li D, Zhang R (2015) Insight into the mechanism of methane synthesis from syngas on a Ni (111) surface: a theoretical study. RSC Adv 5(82):66742–66756
155. Epstein PS, Plesset MS (1950) On the stability of gas bubbles in liquid-gas solutions. J Chem Phys 18(11):1505–1509
156. Hobbs S (1976) Bubble growth in thermoplastic structural foams. Polym Eng Sci 16(4):270–275
157. Song S, Hao Z, Dong L, Li J, Fang Y (2016) A bubble-based EMMS model for pressurized fluidization and its validation with data from a jetting fluidized bed. RSC Adv 6(112):111041–111051
158. Han CD, Yoo HJ (1981) Studies on structural foam processing. IV. Bubble growth during mold filling. Polym Eng Sci 21(9):518–533
159. Papanastasiou AC, Scriven LE, Macosko CW (1984) Bubble growth and collapse in viscoelastic liquids analyzed. J Non-Newtonian Fluid Mech 16(1):53–75
160. Amon M, Denson CD (1984) A study of the dynamics of foam growth: analysis of the growth of closely spaced spherical bubbles. Polym Eng Sci 24(13):1026–1034
161. Amon M, Denson CD (1986) A study of the dynamics of foam growth: Simplified analysis and experimental results for bulk density in structural foam molding. Polym Eng Sci 26(3):255–267
162. Brujan EA (1999) A first-order model for bubble dynamics in a compressible viscoelastic liquid. J Non-Newtonian Fluid Mech 84(1):83–103
163. Joshi K, Lee JG, Shafi MA, Flumerfelt RW (1998) Prediction of cellular structure in free expansion of viscoelastic media. J Appl Polym Sci 67(8):1353–1368
164. Venerus DC, Yala N, Bernstein B (1998) Analysis of diffusion-induced bubble growth in viscoelastic liquids. J Non-Newtonian Fluid Mech 75(1):55–75
165. Otsuki Y, Kanai T (2005) Numerical simulation of bubble growth in viscoelastic fluid with diffusion of dissolved foaming agent. Polym Eng Sci 45(9):1277–1287
166. Agarwal US (2002) Simulation of bubble growth and collapse in linear and pom-pom polymers. e-Polymers 2(1):013
167. Lee JG, Flumerfelt RW (1996) A Refined Approach to Bubble Nucleation and Polymer Foaming Process: Dissolved Gas and Cluster Size Effects. J Colloid Interface Sci 184(2):335–348
168. Kim KY, Kang SL, Kwak HY (2004) Bubble nucleation and growth in polymer solutions. Polym Eng Sci 44(10):1890–1899
169. Shafi MA, Joshi K, Flumerfelt RW (1997) Bubble size distributions in freely expanded polymer foams. Chem Eng Sci 52(4):635–644
170. Goel SK, Beckman EJ (1995) Nucleation and growth in microcellular materials: supercritical CO_2 as foaming agent. AlChE J 41(2):357–367
171. Feng JJ, Bertelo CA (2004) Prediction of bubble growth and size distribution in polymer foaming based on a new heterogeneous nucleation model. J Rheol 48(2):439–462
172. Antunes M, Velasco JI, Realinho V, Martinez AB, Rodríguez-Pérez MÁ, de Saja JA (2009) Heat Transfer in Polypropylene-Based Foams Produced Using Different Foaming Processes. Adv Eng Mater 11(10):811–817
173. Wang J, Zhai W, Ling J, Shen B, Zheng W, Park CB (2011) Ultrasonic Irradiation Enhanced Cell Nucleation in Microcellular Poly(lactic Acid): A Novel Approach to Reduce Cell Size Distribution and Increase Foam Expansion. Ind Eng Chem Res 50(24):13840–13847
174. Richards E, Rizvi R, Chow A, Naguib H (2008) Biodegradable Composite Foams of PLA and PHBV Using Subcritical CO_2. J Polym Environ 16(4):258–266
175. Qiu Y, Lv Q, Wu D, Xie W, Peng S, Lan R, Xie H (2018) Cyclic tensile properties of the polylactide nanocomposite foams containing cellulose nanocrystals. Cellulose 25(3):1795–1807
176. Zhou C, Wang P, Li W (2011) Fabrication of functionally graded porous polymer via supercritical CO_2 foaming. Compos B Eng 42(2):318–325
177. Guo H, Kumar V (2015) Some thermodynamic and kinetic low-temperature properties of the PC-CO_2 system and morphological characteristics of solid-state PC nanofoams produced with liquid CO_2. Polymer 56:46–56
178. Goel SK, Beckman EJ (1994) Generation of microcellular polymeric foams using supercritical carbon dioxide. II: Cell growth and skin formation. Polym Eng Sci 34(14):1148–1156
179. Costeux S, Zhu L (2013) Low density thermoplastic nanofoams nucleated by nanoparticles. Polymer 54(11):2785–2795
180. Yang J, Huang L, Zhang Y, Chen F, Zhong M (2013) Mesoporous silica particles grafted with polystyrene brushes as a nucleation agent for polystyrene supercritical carbon dioxide foaming. J Appl Polym Sci 130(6):4308–4317
181. Zhang C, Zhu B, Li D, Lee LJ (2012) Extruded polystyrene foams with bimodal cell morphology. Polymer 53(12):2435–2442
182. Larsen Å, Neldin C (2013) Physical extruder foaming of poly (lactic acid)-processing and foam properties. Polym Eng Sci 53(5):941–949
183. Zhang C, Zhu B, Lee LJ (2011) Extrusion foaming of polystyrene/carbon particles using carbon dioxide and water as co-blowing agents. Polymer 52(8):1847–1855
184. Okolieocha C, Köppl T, Kerling S, Tölle FJ, Fathi A, Mülhaupt R, Altstädt V (2015) Influence of graphene on the cell morphology and mechanical properties of extruded polystyrene foam. J Cell Plast 51(4):413–426
185. Wang J, Zhu W, Zhang H, Park CB (2012) Continuous processing of low-density, microcellular poly(lactic acid) foams with controlled cell morphology and crystallinity. Chem Eng Sci 75:390–399
186. Li J, Chen Z, Wang X, Liu T, Zhou Y, Luo S (2013) Cell morphology and mechanical properties of microcellular mucell® injection molded polyetherimide and polyetherimide/fillers composite foams. J Appl Polym Sci 130(6):4171–4181
187. Guo MC, Heuzey MC, Carreau PJ (2007) Cell structure and dynamic properties of injection molded polypropylene foams. Polym Eng Sci 47(7):1070–1081
188. Yuan M, Song Q, Turng LS (2007) Spatial orientation of nanoclay and crystallite in microcellular injection molded polyamide-6 nanocomposites. Polym Eng Sci 47(6):765–779
189. Yuan M, Winardi A, Gong S, Turng LS (2005) Effects of nano-and micro-fillers and processing parameters on injection-molded microcellular composites. Polym Eng Sci 45(6):773–788
190. Kramschuster A, Cavitt R, Ermer D, Chen Z, Turng LS (2005) Quantitative study of shrinkage and warpage behavior for microcellular and conventional injection molding. Polym Eng Sci 45(10):1408–1418
191. Chandra A, Gong S, Turng L-S, Gramann P (2004) Cell development in microcellular injection molded polyamide-6 nanocomposite and neat resin. J Cell Plast 40(5):371–382
192. Yuan M, Turng L-S, Gong S, Winardi A, Caulfield D (2004) Crystallization behavior of polyamide-6 microcellular nanocomposites. J Cell Plast 40(5):397–409
193. Yuan M, Turng LS, Caulfield DF (2006) Crystallization and thermal behavior of microcellular injection-molded polyamide-6 nanocomposites. Polym Eng Sci 46(7):904–918
194. Pilla S, Kramschuster A, Yang L, Lee J, Gong S, Turng L-S (2009) Microcellular injection-molding of polylactide with chain-extender. Mater Sci Eng, C 29(4):1258–1265

195. Pilla S, Kramschuster A, Lee J, Clemons C, Gong S, Turng L-S (2010) Microcellular processing of polylactide-hyperbranched polyester-nanoclay composites. J Mater Sci 45:2732–2746
196. Hwang SS, Hsu PP, Yeh JM, Chang KC, Lai YZ (2009) The mechanical/thermal properties of microcellular injection-molded poly-lactic-acid nanocomposites. Polym Compos 30(11):1625–1630